

Bound Roton Pairs in Superfluid Helium*

A. Zawadowski

Department of Physics, University of Virginia, Charlottesville, Virginia 22901

and

Central Research Institute for Physics, Budapest 114, P.O.B. 49, Hungary[†]

and

J. Ruvalds and J. Solana

Department of Physics, University of Virginia, Charlottesville, Virginia 22901

(Received 26 April 1971)

It has recently been proposed that several anomalous features in Raman and neutron scattering experiments on superfluid helium can be explained by the formation of two-roton bound states. In the present paper we analyze in detail the structure in the superfluid helium excitation spectrum associated with bound roton pairs and propose further experiments to examine the nature of the bound states. The two-roton spectrum is calculated including roton-roton interactions over a wide momentum range, and exhibits structure due to bound states which is in remarkable agreement with experiment. Interaction of the two-roton bound state with the single-particle excitations results in a hybridization of these states and a consequent splitting of the single-particle spectrum into two branches; the calculated momentum dependence of these branches is consistent with the neutron data. Inclusion of a finite roton lifetime is shown to be essential to the interpretation of the experimentally observed excitation spectrum in the vicinity of the bound-state energy. Possible physical mechanisms for the roton-roton interaction are considered, and the angular momentum character of the bound states is briefly discussed.

I. INTRODUCTION

Following the pioneering work of Landau¹ some thirty years ago, there has been considerable experimental and theoretical interest² in the excitation spectrum of superfluid helium. To explain the peculiar thermodynamic properties of liquid helium, Landau proposed that the excitation spectrum is of the form shown in Fig. 1; i. e., he suggested that the spectrum consists of phononlike excitations at small momenta plus a new type of excitation (rotons) corresponding to the energy minimum in the dispersion curve. Many of the physical properties of liquid helium, such as the viscosity, are a direct consequence of the presence of these excitations and consequently exhibit a temperature dependence which can be related to the form of the dispersion curve shown in Fig. 1. For low temperatures, only a few excitations are present, and they behave much like a gas. Thus, early treatments of the thermodynamic properties based on kinetic theory were reasonably successful.

Landau and Khalatnikov^{3,4} (LK) first considered roton-roton interactions in an attempt to explain the roton contribution to the viscosity of liquid He II. Lacking a theoretical understanding of the nature of their interactions, or even the physical nature of rotons, LK chose to represent the roton-roton scattering by a simple δ -function interaction of the form $V_0 \delta(\vec{r}_1 - \vec{r}_2)$, where V_0 is constant and \vec{r}_1 denotes the position of a roton. To within avail-

able experimental accuracy, the LK theory was remarkably successful in explaining a temperature-independent roton contribution to the viscosity. However, the experimental data were taken over a limited temperature range, so that the temperature dependence of the viscosity cannot be considered as completely confirmed. In essence the experimental data, albeit limited, suggest that the roton lifetime is limited primarily by collision broadening from other rotons and therefore is inversely proportional to the number of rotons. Furthermore, comparison of the LK theory with viscosity data gives an estimate⁴ for the roton-roton interaction strength of $|V_0| = 2.63 \times 10^{-38}$ erg cm³.

The theoretical understanding of the superfluid helium excitation spectrum was placed on a more fundamental foundation based on quantum mechanics by the works of Feynman and Cohen.^{5,6} By means of a variational calculation,⁵ Feynman and Cohen were able to derive from first principles the excitation spectrum shown by dotted lines in Fig. 2. Thus the latter theories verified the qualitative nature of the superfluid helium dispersion curve proposed by Landau and furthermore suggested that rotons behave like quantum-mechanical analogs of smoke rings. The above derivation of the excitation spectrum does not include roton-roton interactions. If we visualize rotons as modified free particle excitations which are moving surrounded by a backflow of other helium atoms, i. e., a description reminiscent of classical smoke rings, then it is

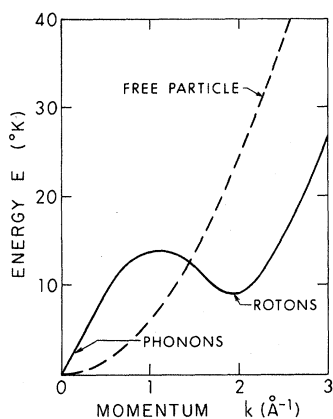


FIG. 1. The excitation spectrum of superfluid helium proposed by Landau is shown by the solid line. The Landau spectrum exhibits a minimum corresponding to roton excitations in marked contrast to the free helium particle spectrum indicated by the dotted curve.

clear that the true roton-roton interaction is likely to be very complicated and may depend on the relative orientations of the rotons. Nevertheless, Cohen and Feynman⁶ have shown that the roton-roton interaction includes a component arising from the possible process of one roton emitting a phonon which is then absorbed by another roton. The latter process can be treated in the so-called deformation potential approach which is valid only for small momentum transfer. Assuming that the latter mechanism dominates the roton-roton interaction, and neglecting momentum-dependent terms in the coupling,⁷ the coupling parameter V_0 can be independently estimated from the dependence of the roton energy on the external pressure⁸ and is found to be $V_0 = -1.3 \times 10^{-38}$ erg cm³.⁵

Vigorous experimental efforts, especially by means of neutron scattering, have yielded very precise information on the nature of the excitation spectrum of He II and verified several features of the dispersion curve shown in Fig. 1.⁹ On the other hand, new theoretical as well as experimental developments suggested that the dispersion curve for superfluid helium was in fact more complicated. Pitaevskii¹⁰ argued, using elegant field theory techniques, that the excitation spectrum should bend over at an energy near $2\Delta_0$, where Δ_0 is the roton energy. He reasoned that the dispersion curve should terminate at $2\Delta_0$ and at this energy the dispersion curve should have a horizontal tangent of infinite order associated with an instability of single-particle excitations toward decay into two rotons. Such a "bend" in the spectrum at an energy near $2\Delta_0$ was demonstrated by neutron scattering experiments,^{9,11} but seems to occur at an energy *larger* than $2\Delta_0$ in contrast to Pitaevskii's

theoretical prediction. It is important to note that Pitaevskii's treatment neglects the influence of a finite roton lifetime.

Recent neutron scattering data¹¹ on helium have revealed anomalous structure in the excitation spectrum as shown in Fig. 2. An especially peculiar feature of the experimental results shown in Fig. 2 is the existence of two distinct branches in the single-excitation spectrum which remained anomalous in terms of previous theories.

With the advent of laser technology, light scattering experiments have proven to be an extremely powerful probe of the excitation spectrum. Greytak and Yan¹² contributed considerably to our understanding of the excitation spectrum by observing the Raman spectrum of superfluid helium as a function of temperature. In Raman processes the wave vector of the light is much smaller than the roton momentum; consequently the light interacts only with roton pairs whose total momentum is approximately zero. The theory of the scattering process has been worked out by Stephen¹³ and is successful in explaining many features of the Raman experiments. On the basis of the existence of sharp peaks in the joint density of states (involving two excitations), the Stephen theory predicts two peaks in the Raman spectrum at energies $2\Delta_0$ and

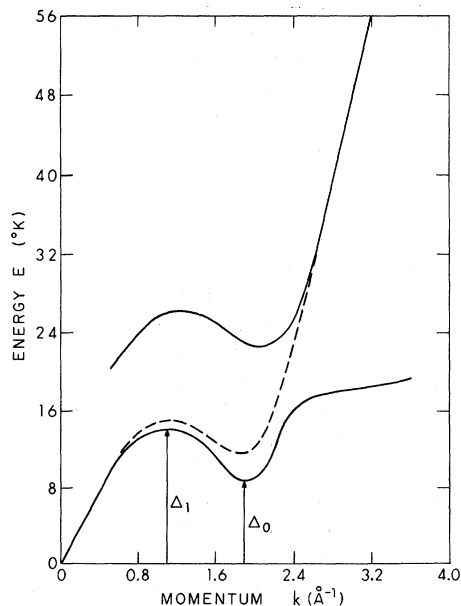


FIG. 2. The excitation spectrum as derived by Feynman and Cohen (dotted curve), and the excitation spectrum obtained from neutron scattering experiments of Ref. 11 (solid lines). Note that the experimental results show the existence of two branches in the spectrum with a peculiar dispersion in the vicinity of $2\Delta_0$. The neutron data taken at $T = 1.1^\circ\text{K}$ yield the following parameters: $\Delta_0 = 8.65^\circ\text{K}$, $\Delta_1 = 13.9^\circ\text{K}$, $k_0 = 1.91 \text{ \AA}^{-1}$, $k_1 = 1.1 \text{ \AA}^{-1}$, $\mu_0 = 1.06 \times 10^{-24}$ g, and $\mu_1 = 3.3 \mu_0$.

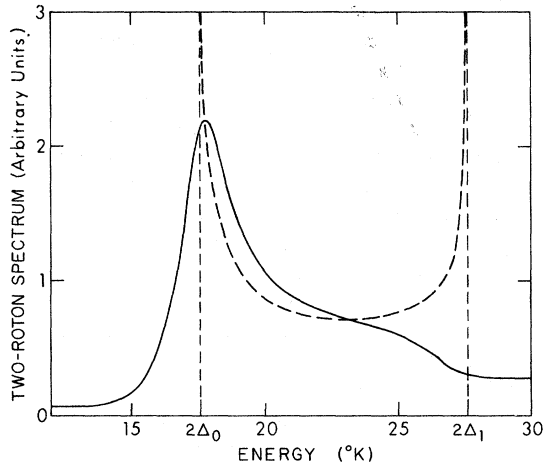


FIG. 3. Density of states as a function of energy for two rotors with zero total momentum. The dotted lines show the singularities in the density of states in the absence of interactions between excitations. The solid curve is the experimental spectrum of liquid helium taken from the Raman data of Ref. 12.

$2\Delta_1$, respectively (see Fig. 3). Greytak and Yan's experimental results¹² were especially startling since only a single peak was observed at an energy nearly twice the single-roton energy, as shown by the solid curve in Fig. 3.

The anomalous peak structure in the Raman data, as well as the peculiar splitting of the excitation spectrum observed by neutron scattering, were explained by the existence of bound states in the two-roton system by Ruvalds and Zawadowski.¹⁴ Assuming that the roton-roton interaction is attractive, as suggested by the phonon-mediated scattering mechanisms,⁸ a bound state of two rotors can be split off below the continuum at an energy $\epsilon = 2\Delta_0 - E_b$, where E_b is the binding energy. By means of extremely precise techniques Greytak has recently measured the binding energy E_b and consequently confirmed experimentally the existence of two-roton bound states with zero total momentum.¹⁵ The possibility of forming two-roton resonances with total momentum zero has been demonstrated independently by Iwamoto¹⁶ using a phase shift analysis of the scattering amplitude for two rotors coupled by a separable potential.

In the present paper we consider in detail the formation of bound states of two rotors and calculate the roton spectrum for a wide range of momenta. For the limiting case of infinite single-roton lifetime, corresponding to zero temperature, we give analytic expressions for the spectrum which exhibit sharp peaks corresponding to a two-roton bound state which is formed by arbitrarily weak roton-roton coupling. In the weak-coupling limit, the binding energy is calculated for bound roton

pairs with zero, as well as finite, total momentum. The fact that bound states of two rotors can be split off below the two-roton continuum by arbitrarily weak coupling is related to the form of the unperturbed density of states $\rho_2^{(0)}(\epsilon)$: In the $K=0$ case, $\rho_2^{(0)}(\epsilon)$ has a square root singularity, whereas for finite K the density of states has a threshold in energy at twice the single-roton energy. The present calculations are based on a model Hamiltonian representing the roton-roton interaction as arising from a phonon-exchange mechanism. We show that the analysis of the spectrum in terms of generalized coupling g_l , where l refers to the angular momentum character of the roton pair, yields the same energy dependence for the spectrum as obtained by using a δ -function model for the interaction.

An essential feature in the calculation of the two-roton spectrum is the inclusion of the single-roton lifetime which is induced by collision broadening. If the roton energy width becomes comparable to the binding energy of the two-roton bound state, then it is more appropriate to discuss the spectrum in terms of two-roton resonances near the bottom of the continuum. Presently available experimental data are in a temperature range where the collision-induced width is in fact comparable to the binding energy; thus many features of the observed spectrum, especially the temperature dependence of the roton lifetime, are difficult to interpret in terms of previous theories. In fact, a primary motivation of the present work was to resolve the discrepancy in the strength of the roton-roton coupling obtained from the Raman data, as opposed to estimates from viscosity data.^{4,14} The above estimates of the roton-roton interaction differ by an order of magnitude.¹⁴ In an attempt to resolve the above discrepancy we have gone beyond the Landau and Khalatnikov theory of the roton lifetime, which was based on second-order perturbation theory, and include the changes in the single-roton lifetime due to two-roton resonances. The latter analysis will be discussed in a forthcoming publication.

We employ Green's function techniques as they are ideally suited for our purposes, especially since they provide a natural way to include the collision-induced single-roton lifetime in the calculation, and demonstrate explicitly the structure in the spectrum due to coupled roton pairs.

Other examples of bound states and resonances of two excitations are given by two-magnon bound states¹⁷ in Heisenberg ferromagnets and bound phonon pairs in crystals.¹⁸

Rather dramatic effects are expected whenever the energy of a bound state is nearly degenerate with the energy of another excitation. Under these circumstances a hybridization of excitations is pos-

sible which exhibits the general phenomena of level repulsion in quantum mechanics. Such hybridization processes have been considered for a variety of physical systems. The first instance of level repulsion between a single-quantum state and the "overtone" of another state was suggested by Fermi¹⁹ to explain the anomalous Raman spectrum of CO₂ in terms of molecular vibration theory. Hybridization of two-magnon bound states with single-magnon excitations has been demonstrated theoretically²⁰ and the analogous mixing of phonon excitations in solids has been analyzed both experimentally²¹ and theoretically.²² The hybridization can strongly modify the single-excitation spectrum even if the resonance is not near in energy to the single excitation, providing that the hybridization interaction is quite strong, as in the case of phonon interactions in the highly anharmonic quantum crystals.²³ Similarly, in the case of liquid helium, we shall see that formation of bound roton pairs will strongly renormalize the single-roton states.

It has been suggested¹⁴ that a hybridization of single-particle states with a two-roton bound state in superfluid helium would split the single-particle spectrum into two branches in a manner similar to experimental results shown in Fig. 2. In the present paper we calculate the above hybridization process over a large momentum interval and make a detailed comparison of our theoretical spectrum with the neutron scattering data. Our results indicate that the hybridization process can give rise to an unusual temperature dependence for the single-particle spectrum which should be observable by neutron scattering experiments at lower temperatures.

It is very important to note that the interpretation of the two branches in the excitation spectrum shown in Fig. 2 as a consequence of the above hybridization process involving two-roton bound states with finite momentum,¹⁴ indicates that the proper unrenormalized single-particle spectrum for superfluid helium should be of the form proposed by Landau¹ and derived by Feynman and Cohen⁵; i.e., the unperturbed dispersion curve has a continuous momentum dependence as shown by the dotted curve in Fig. 2. Thus the *unrenormalized* spectrum does not include the so-called "plateau" region of the lower dispersion branch which is a result of the roton coupling. The above distinction is vital in understanding the experimental results. Some theories which treat the *unperturbed* single-particle spectrum as consisting of two distinct branches predict spurious results; e.g., additional peaks with considerably large intensity in the Raman spectrum associated with the "plateau" region,¹⁶ and extra branches in the dispersion curve²⁴ which are *not* observed experimentally. It would be desirable to develop a theory which includes the

"plateau" regions as well as the higher anomalous branch in a truly self-consistent calculation of the two-roton spectrum. However such a self-consistent analysis is beyond the scope of the present paper.

Concerning the existence of two branches in the He spectrum we should mention Iwamoto's recent work²⁵ discussing the problem independently. In his calculation of the He spectrum the one- and two-excitation intermediate states have been considered, so that the existence of the two branches has been undoubtedly shown; he started from first principles, however his results give a gross behavior of the dispersion of the two branches which bears little resemblance to experiment. Also, Soda, Sawada, and Nagaya²⁶ have discussed the sum rules of the He spectrum by accepting the existence of the second branch on experimental grounds.¹¹ Their work assumes that the upper branch is a two-phonon state which is completely independent of the single-phonon states and has an infinite lifetime.²⁶ Since the upper branch is well within the two-roton continuum and hybridizes with the single-particle spectrum, the latter approximations do not seem to be consistent with the neutron data.¹¹ Finally we emphasize once more the necessity of including roton lifetime effects in interpreting the experimental neutron data. The fact that rotons have a finite lifetime can produce a temperature dependence of the structure associated with bound roton pairs. In the present paper we demonstrate the strong influence of the roton lifetime on the spectrum, particularly near the hybridization region, and thereby resolve the anomaly concerning the position of the lower branch of the single-particle spectrum which lies above $2\Delta_0$ according to neutron data in contrast to previous theoretical predictions.^{24,10}

The present paper is organized in the following manner. The mathematical formulation of the problem is presented in Sec. II. A detailed analysis of the formation of two-roton bound states is given in Sec. III for momenta $K=0$ (related to the Raman scattering spectrum) and $K \neq 0$ as well. The results of Sec. II B are extended in Sec. IV to treat the hybridization of the bound state with single-particle states. Possible physical mechanisms for the roton-roton interaction and some conclusions drawn from the present study are discussed in Secs. V and VI.

II. FORMULATION OF PROBLEM

The basic theme of our theory is to consider the superfluid helium excitation spectrum in two steps. First we suppose that the quasiparticle excitation spectrum in the absence of interactions between quasiparticles is of the form proposed by Landau¹ and later derived by Feynman and Cohen⁵ using a

variational calculation. Thus the unrenormalized dispersion curve is a continuous function of momentum and exhibits an energy minimum corresponding to roton excitations as shown in Fig. 1. The second step is to introduce interactions between quasiparticles and study the modifications in the spectrum due to the coupling between rotons, i. e., quasiparticles corresponding to the neighborhood of the energy minimum. Our approach is analogous to the scheme employed by Cohen and Feynman⁶ and Pittaevskii¹⁰ to study the helium spectrum.

We choose to express the formalism in terms of the mathematical framework developed by Belyaev,^{27,28} and previously applied by Pittaevskii.¹⁰ Thus we apply standard diagrammatic techniques for particles with finite momentum and consider the condensate of zero-momentum particles as a kind of external field. We introduce helium particle field operators $\psi(\vec{r}, t)$ in the Heisenberg representation. These ψ operators are related to the boson destruction operators in the usual way:

$$\psi(r, t) = (2\pi)^{-3/2} \int d^3k a_k(t) e^{i\vec{k}\cdot\vec{r}}. \quad (2.1)$$

It is important to stress that our description is quite different from theories which treat the excitation spectrum in terms of different products of density fluctuation operators in the interaction representation.²⁷

As the energies of interest in the roton spectrum are much larger than the relevant temperatures, we employ zero-temperature Green's function techniques in most of the present paper and consider the roton lifetime as a temperature-dependent parameter. However, in a subsequent paper, we calculate the roton lifetime using thermodynamic Green's function techniques to obtain a thorough check on the validity of our approximations for the roton lifetime.

A unique feature of superfluid helium is the existence of a large number of particles with zero momentum (condensed phase). It is convenient to separate operators ξ_0 for particles in the condensate by introducing new field operators $\psi' = \psi - \xi_0$ as discussed in Refs. 27 and 28. The single-particle causal Green's function is then defined in terms of helium particle field operators as

$$G_1(x - x', t - t') = -\langle T \{ \psi'(x, t) \psi'^{\dagger}(x', t') \} \rangle, \quad (2.2)$$

where T is a time ordering operator. The corresponding Fourier transformed propagator is

$$G_1(k, \omega) = \int d^3x dt G_1(x, t) e^{-i(kx - \omega t)}. \quad (2.3)$$

In the spirit of our approach we suppose that the zero-order Green's function includes all of the physical information needed to describe the Landau excitation spectrum shown in Fig. 1. In other words, we consider the single-particle Green's function to be of the form

$$G_1^{(0)} = \frac{Z_1(k)}{\omega - E(k) + \frac{1}{2}i\Gamma} \approx \frac{1}{\omega - E(k) + \frac{1}{2}i\Gamma}, \quad (2.4)$$

where $Z_1(k)$ is a normalization factor, $E(k)$ is the energy spectrum given in Fig. 1, and Γ is the single-particle width which is assumed to be independent of energy and momentum but may be temperature dependent. The Green's function written in Eq. (2.4) neglects a second term with energy denominator $\omega + E(k) - \frac{1}{2}i\Gamma$ which contributes only a small correction providing $kT \ll E(k)$. In the absence of information relating to the normalization factor Z_1 , we choose Z_1 to be unity for convenience. This assumption seems to be a good approximation for large enough momentum k . At small momenta, $Z_1(k)$ is strongly momentum dependent²⁸: This dependence is important in satisfying the sum rules.^{29,30} It is worth mentioning that the approximate form of G_1 in Eq. (2.4) is based on the assumption that the Green's function defined in terms of helium particle operators [see Eq. (2.2)] exhibits a strong pole at the quasiparticle energy.

Turning now to the problem of interactions between quasiparticles we write the two-particle coupling in the general form

$$\mathfrak{H}_{\text{int}} = \frac{1}{2}(2\pi)^{-3} \int a_{k_1}^{\dagger} a_{k_2}^{\dagger} \gamma(k_1 k_2 k_3 k_4) a_{k_3} a_{k_4} d^3k_1 \cdots d^3k_4, \quad (2.5)$$

where the irreducible vertex function γ describes the correct interaction between two quasiparticles in the two-particle-two-particle channel and may be strongly momentum dependent.⁶ We construct a model Hamiltonian by making the replacement

$$\gamma(k_1 k_2 k_3 k_4) \rightarrow g_4 \delta(k_1 + k_2 - k_3 - k_4), \quad (2.6)$$

where g_4 is a coupling constant. This approximation assumes a point interaction, i. e., a δ -function interaction in real space, and yields a model Hamiltonian of the form

$$\mathfrak{H}_{\text{int}} = \frac{1}{2} g_4 \int \psi'^{\dagger}(x) \psi'^{\dagger}(x) \psi'(x) \psi'(x) d^3x. \quad (2.7)$$

Of course, in order to use the model in various regions of momentum space, different values of g_4 should be used in different momentum intervals.

In the case of interacting rotons with total momentum zero, the interaction term g_4 couples only s -like states. The extension of our model to coupling of states with other angular momenta is straightforward and is carried out in Sec. III.

The one-particle density of states ρ_1 is related in a simple way to the imaginary part of the G_1 propagator, i. e.,

$$\rho_1(k, \omega) = -(1/\pi) \text{Im} G_1(k, \omega + i\delta). \quad (2.8)$$

To consider two-roton resonances we need to calculate the two-particle Green's function

$$G_2(x - x', t - t')$$

$$= -i \langle T \{ \psi'(x, t) \psi'(x, t) \psi'^{\dagger}(x', t') \psi'^{\dagger}(x', t') \} \rangle, \quad (2.9)$$

and thus obtain the two-particle density of states

$$\rho_2(K, \omega) = -(1/4\pi) \text{Im} G_2(K, \omega + i\delta), \quad (2.10)$$

where K denotes the total momentum of the pair, ω is the total energy, and $G_2(K, \omega)$ is the Fourier transform [as in Eq. (2.3)] of the two-particle propagator defined in Eq. (2.9). If a bound state of two rotons can occur, it will be manifested by a pole in the two-particle Green's function. Raman scattering experiments measure the two-particle density of states $\rho_2(K=0, \omega)$ and consequently exhibit directly the structure in the spectrum associated with two-roton bound states.

As pointed out in the Introduction, the existence of a bound roton pair can modify the single-particle spectrum in an essential way. The physical process which dominates the interaction between one- and two-particle states is illustrated diagrammatically in Fig. 4(a); i. e., a single particle interacting with a zero-momentum condensate particle can be transformed into a two-particle excitation such as a bound roton pair. The interaction Hamiltonian for the latter coupling process can be extracted from the general vertex function by writing the contributions of the condensate coupling as

$$\begin{aligned} \gamma_c(k_1 k_2; k_3 k_4) &= \delta(k_4) \gamma_3(k_1 k_2; k_3) + \delta(k_3) \gamma_3(k_1 k_2; k_4) \\ &+ \delta(k_1) \gamma_3^*(k_2; k_3 k_4) + \delta(k_2) \gamma_3^*(k_1; k_3 k_4), \end{aligned} \quad (2.11)$$

where the δ function refers to a particle in the zero-momentum condensate and the vertex function γ_3 can be expressed in terms of our model Hamiltonian:

$$\begin{aligned} \gamma_3(k_1 k_2; k_3) &= g_3(T) \delta(k_1 + k_2 - k_3) \\ &= g_4 [N_0(T)]^{1/2} \delta(k_1 + k_2 - k_3), \end{aligned} \quad (2.12)$$

where $N_0(T)$ is the temperature-dependent number of particles in the condensate. By writing $g_3(T) = g_4 [N_0(T)]^{1/2}$, we are treating the creation and destruction operators ξ_0^\dagger and ξ_0 for condensate particles as c numbers, i. e., $\xi_0 \rightarrow [N_0(T)]^{1/2}$, in the usual manner.^{27, 28} Hence we represent the interaction between one- and two-particle states by the model Hamiltonian

$$\mathcal{H}_3 = g_3 \int \psi'^{\dagger}(x) \psi'(x) \psi'(x) + \text{c. c.} \quad (2.13)$$

To include interactions between excitations in the calculation of the spectrum, we apply diagrammatic techniques using the unrenormalized propagators defined in Eq. (2.4) and represented by solid lines in our diagrams. Condensate particles are denoted by zig-zag lines as in Fig. 4(a). Note that the unrenormalized spectrum $[E(k)$ in Eq. (2.4)]

consists of a single continuous branch as shown in Fig. 1, in contrast to the experimentally observed two-branch spectrum of Fig. 2. Interactions between excitations are represented by the model Hamiltonians given by Eqs. (2.7) and (2.12), with the coupling coefficients g_4 and g_3 considered as adjustable parameters which are related to the quasi-particle vertex function in various momentum regions. The zero-momentum condensate propagator (zig-zag line) has only one connection to the diagram vertices since it is represented by a c number.

The above formalism will be applied first to study the formation of two-roton bound states by calculating the two-particle Green's function including interactions given by the \mathcal{H}_4 Hamiltonian. We then use the renormalized two-particle Green's functions (including interactions) together with the \mathcal{H}_3 model Hamiltonian to study the mixing of single-particle excitations with the bound state. The mixing splits the single-particle spectrum into two components in agreement with experiment.

In a subsequent article, the present formalism is extended to finite temperature techniques using thermodynamic Green's functions in order to derive the temperature dependence of the single-roton lifetime.

III. TWO-ROTON BOUND STATES

To examine the structure of two-roton bound states we restrict attention to the energy region extending from the bottom of the roton minimum Δ_0 to the local maximum Δ_1 shown in Fig. 2. Hence we treat the roton-roton scattering as a two-body problem, since the contributions from coupling to small- q phonons are not taken explicitly into account and the population of the roton states is small in the temperature range of interest. As pointed out by Feynman and Cohen,⁶ the phonon exchange

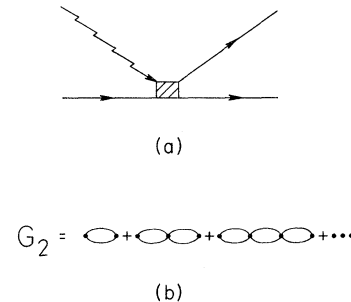


FIG. 4. (a) Diagrammatic representation of the interaction responsible for the hybridization of the single-particle spectrum with two-roton bound states. Solid lines indicate single-particle excitations (e.g., rotons), whereas the zig-zag line represents a particle from the condensate. (b) Bethe-Salpeter equation for two-roton propagator G_2 .

process is important in the roton-roton scattering; in our treatment these processes are considered by means of an effective roton-roton coupling.

The scattering process can be expressed in terms of a Bethe-Salpeter equation for the two-particle Green's function which is obtained by summing the diagrams in Fig. 4(b). The corresponding Green's function equation is given by

$$G_2(x-x') = 2i \{ [G_1^{(0)}(x-x')]^2 + ig_4 \int d^4x'' [G_1^{(0)}(x-x'')]^2 \times [G_1^{(0)}(x''-x')]^2 + \dots \}. \quad (3.1)$$

The factor of 2 outside the bracket arises because of ordering of field operator pairings as required by Wick's theorem.²⁸ The theoretical development is greatly simplified by writing a single diagram loop as

$$F(x-x') = i[G_1^{(0)}(x-x')]^2, \quad (3.2)$$

and, following the prescription of Eq. (2.3), obtaining the Fourier transform of the loop

$$F(K, \omega) = [i/(2\pi)^4] \int d^3k \int d\tilde{\omega} G_1^{(0)}(k, \tilde{\omega}) \times (K-k, \omega-\tilde{\omega}) G_1^{(0)}(k, \tilde{\omega}), \quad (3.3)$$

in terms of the propagators $G_1^{(0)}(k, \omega)$ defined in Eq. (2.3). Then it is a straightforward task to Fourier transform the series in Eq. (3.1) and sum the resulting geometric series to obtain the two-particle Green's function including interactions

$$G_2(K, \omega) = 2F(K, \omega)/[1 - g_4 F(K, \omega)]. \quad (3.4)$$

From the above simple expression for the Green's function, the two-roton density of states follows immediately and is given by

$$\rho_2(K, \omega) = -(1/4\pi) \text{Im} G_2(K, \omega) \\ = -\frac{1}{2\pi} \left(\frac{\text{Im} F}{[1 - g_4 \text{Re} F]^2 + [g_4 \text{Im} F]^2} \right), \quad (3.5)$$

in terms of the real and imaginary parts of the F function defined in Eq. (3.4). The factor of $\frac{1}{4}$ in Eq. (3.5) comes from two factors: One $\frac{1}{2}$ is due to the possible pairings of the field operators while another $\frac{1}{2}$ takes into account the indistinguishability of Bose particles. Incidentally, a simple check of the factors in Eq. (3.5) is to substitute the two-particle Green's function [Eq. (3.4)] in the limit of zero interactions, into Eq. (3.5) to obtain the unrenormalized density of states. Taking the single-particle states as noninteracting excitations with infinite lifetimes ($\Gamma=0$), the joint density of states $\rho_2^{(0)}$ follows from Eqs. (3.3)–(3.5) using the unrenormalized propagators of Eq. (2.4):

$$\rho_2^{(0)}(K, \omega) = \frac{1}{2(2\pi)^3} \int d^3k \delta(\omega - \epsilon_k - \epsilon_{K-k}), \quad (3.6)$$

where the $\frac{1}{2}$ factor is again related to the indistin-

guishability of rotons. Inclusion of the finite single-roton lifetime is vital to our analysis and can be done by evaluating Eq. (3.3) with unperturbed Green's functions [Eq. (2.3)] containing a phenomenological width Γ to obtain

$$F(K, \omega) = 2 \int \frac{\rho_2^{(0)}(K, \omega') d\omega'}{\omega - \omega' + i\Gamma}, \quad (3.7)$$

where $\rho_2^{(0)}$ is given in Eq. (3.6). It is apparent then that the unperturbed density of states $\rho_2^{(0)}$ plays a key role in determining the character of the full two-particle Green's function including interactions. The computation of $\rho_2^{(0)}(K, \omega)$ is somewhat tedious and is relegated to the Appendix. Since the spectrum derived in the Appendix displays rather different behavior in different momentum regions, we shall treat the $K=0$ case separately from the $K \sim k_0$ region.

A. Bound States with $K=0$

In Raman scattering experiments the momentum of the light is very small relative to the roton momentum and consequently the light samples only the two-excitation spectrum with total momentum zero. To calculate the two-roton spectrum we consider first bound states with s -like symmetry, i.e., zero total angular momentum, which are coupled by the model Hamiltonian in Eq. (2.7) corresponding to a point interaction. The extension of our analysis to bound states with finite angular momentum involves only a trivial modification of our model Hamiltonian and is carried out at the end of this section.

We begin with a discussion of the spectrum for the idealized case of infinite roton lifetime ($\Gamma=0$) and later proceed to the realistic situation of rotons with finite lifetime.

As the primary energy regions of interest are quite close to the extremal points of the dispersion curve in Fig. 1, it is a good approximation to use a parabolic form of the excitation dispersion:

$$E_{\text{roton}} = \Delta_0 + (k - k_0)^2/2\mu_0, \quad (3.8a)$$

$$E_{\text{max}} = \Delta_1 - (k - k_1)^2/2\mu_1. \quad (3.8b)$$

The energy and momentum parameters (Δ_0 , Δ_1 , k_0 , and k_1) are defined in Fig. 2, and the "effective masses" μ_0 and μ_1 are associated with the roton and "max" excitations. The max label refers simply to the excitations near the Δ_1 local maximum of the dispersion curve.

From the Appendix, the unperturbed two-roton density of states, neglecting terms proportional to the small quantities $(\omega - 2\Delta_0)$ and $(2\Delta_1 - \omega)$, is given by

$$\rho_2^{(0)}(K=0, \omega) = \left(\frac{k_0}{2\pi} \right)^2 \left(\frac{\mu_0}{\omega - 2\Delta_0} \right)^{1/2}$$

$$+ \left(\frac{k_1}{2\pi} \right)^2 \left(\frac{\mu_1}{2\Delta_1 - \omega} \right)^{1/2}. \quad (3.9)$$

The above formula is valid only near the threshold regions $\omega \sim 2\Delta_0$ and $\omega \sim 2\Delta_1$, respectively. It is apparent from Eq. (3.9) that the unrenormalized two-particle density of states exhibits two singularities as shown by the dotted lines in Fig. 3. However, the experimental data for the Raman scattering from liquid helium taken by Greytak and Yan (shown by the solid line in Fig. 3) exhibits only a single peak in the spectrum near twice the roton energy. This anomalous discrepancy between experiment and the unperturbed density of states led to the suggestion that roton-roton interactions could strongly modify the two-roton spectrum.^{14,16}

The influence of roton-roton coupling on the two-roton spectrum is manifested by formation of two-roton bound states and also by broadening of the spectrum associated with the finite roton lifetime. In the present subsection we neglect lifetime effects and, in the interest of clarity, present a calculation of the spectrum only near the two-roton region of energy. Thus, we shall not write down explicitly the contribution from the max energy region ($\omega \sim 2\Delta_1$), but rather demonstrate the changes in the latter part of the spectrum graphically. The two-roton spectrum is obtained by first evaluating the F function from Eq. (3.9); thus

$$F(K=0, E) = 2 \left(\frac{k_0}{2\pi} \right)^2 \mu_0^{1/2} \int_0^{2D} \frac{x^{-1/2} dx}{E - x + i\delta}, \quad (3.10)$$

in terms of convenient variables $x = \omega' - 2\Delta_0$, $E = \omega - 2\Delta_0$, and a cutoff energy $D = \Delta_1 - \Delta_0$. The F function in Eq. (3.10) determines the spectrum within the continuum ($E > 0$) as well as the spectrum associated with bound states at $E < 0$ which are split off below the two-roton continuum by an attractive coupling between excitations.³¹

Below the continuum, i.e., $E < 0$, the integration in Eq. (3.10) is trivial and gives

$$F(K=0, E < 0) = -4(k_0/2\pi)^2 \mu_0^{1/2} |E|^{-1/2} \times \tan^{-1}(|2D/E|^{1/2}) - i\delta \quad (3.11)$$

in the limiting case of δ tending to zero. Now making use of the representation for a δ function $\delta(z) = \lim_{\sigma \rightarrow 0} \pi^{-1} \sigma / (z^2 + \sigma^2)$ in Eq. (3.5), we obtain the density of states below the continuum,

$$\rho_2(K=0, E < 0) = (1/2g_4) \delta[1 - g_4 \text{Re } F(K=0, E < 0)]. \quad (3.12)$$

As in Ref. 14, it is convenient to express the results in dimensionless quantities \hat{f} defined by $F = \frac{1}{2} \hat{\eta} \hat{f}$, with $\hat{\eta} = k_0^2 \pi^{-2} (\mu_0/2D)^{1/2}$; $\epsilon = E/2D = (\omega - 2\Delta_0)/2D$ is a dimensionless energy and $\hat{g}_4 = \frac{1}{2} \hat{\eta} g_4$ denotes a dimensionless coupling constant. In terms of

these dimensionless quantities the density of states is, for $\epsilon < 0$,

$$\rho_2(K=0, \epsilon) = (1/4\hat{g}_4) \hat{\eta} \delta(1 - \hat{g}_4 \text{Re } \hat{f}), \quad (3.13)$$

with

$$\text{Re } \hat{f} = -2|\epsilon|^{-1/2} \tan^{-1}(|\epsilon|^{-1/2}). \quad (3.14)$$

A bound state of two rotons with energy below the continuum exists if the argument of the δ function in Eq. (3.13) vanishes. It is clear, then, from Eq. (3.14) that for attractive coupling ($\hat{g}_4 < 0$) a bound-state solution exists for arbitrarily small values of the coupling! In the weak-coupling limit ($|\epsilon| \ll 1$) the solution for the binding energy [from Eqs. (3.13)–(3.14)] is found to be

$$\epsilon_B = -\pi^2 (\hat{g}_4)^2. \quad (3.15)$$

The fact that a bound state is created by arbitrarily weak coupling is a consequence of the singularity in the unperturbed roton density at the $\epsilon = 0$ threshold. Using Eqs. (3.13) and (3.15), it is possible to write the density of states in the form

$$\rho_2(K=0, \epsilon) = \frac{1}{2} \hat{\eta} |\hat{g}_4| \pi^2 \delta(\epsilon - \epsilon_B), \quad (3.16)$$

which indicates the strength of the peak in the spectrum corresponding to the bound state. It is easy to show, and convincing on physical grounds, that an attractive coupling can never give rise to a bound state of two max quasiparticles above the continuum. Of course if the coupling were repulsive ($\hat{g}_4 > 0$), the situation would be reversed so that a bound state would be formed above the continuum as in the case of bound phonon pairs in solids.¹⁶

Turning now to the continuum energy region $E > 0$, Eq. (3.10) takes the form

$$F(K=0, E > 0) = 2 \left(\frac{k_0}{2\pi} \right)^2 \mu_0^{1/2} \times \left(E^{-1/2} \ln \left| \frac{E^{1/2} + (2D)^{1/2}}{E^{1/2} - (2D)^{1/2}} \right| - i\pi E^{-1/2} \right), \quad (3.17)$$

or, in terms of our dimensionless units,

$$\hat{f}(K=0, \epsilon > 0) = \epsilon^{-1/2} \ln \left| \frac{1 + \epsilon^{1/2}}{1 - \epsilon^{1/2}} \right| - i\pi \epsilon^{-1/2}. \quad (3.18)$$

Substituting the real and imaginary parts of f from Eq. (3.18) into the general expression for the density of states given by Eq. (3.5), we obtain

$$\rho_2(K=0, \epsilon > 0) = -\frac{\hat{\eta}}{4\pi} \frac{\text{Im } \hat{f}}{[1 - \hat{g}_4 \text{Re } \hat{f}]^2 + [\hat{g}_4 \text{Im } \hat{f}]^2}. \quad (3.19)$$

The spectrum given by Eq. (3.19) displays an interesting physical consequence of the excitation coupling which may be observable experimentally at sufficiently low temperatures. Namely, a glance

at the imaginary part of f in Eq. (3.18) shows that the total density of states ρ_2 exhibits a sharp dip near the threshold energies, i. e., the imaginary part of \hat{f} diverges at energy $\epsilon = 0$ which means that the density of states vanishes at the threshold energy. A similar analysis shows that the spectrum must also vanish at $\epsilon = 1$, i. e., at the E_{\max} threshold. In other words, the square root singularities of the unrenormalized density of states at the continuum edges (see Fig. 2) are completely removed by the interactions between excitations. The latter result was previously pointed out by Iwamoto.¹⁶ Furthermore, as a result of the structure in Eqs. (3.18) and (3.19), secondary peaks in the spectrum can appear within the continuum at energies near the threshold edges. To examine the structure in the spectrum within the continuum we substitute Eq. (3.18) into Eq. (3.19) to obtain

$$\rho_2(K=0, \epsilon > 0) = \frac{\hat{\eta}}{4} \frac{\epsilon^{-1/2}}{[1 + \hat{g}_4 \epsilon^{-1/2} \ln |(1 + \epsilon^{1/2}) / (1 - \epsilon^{1/2})|^2 + \pi^2 \epsilon^{-1} \hat{g}_4^2]} \quad (3.20)$$

The spectral function ρ_2 from Eqs. (3.13) and (3.20) is plotted in Fig. 5 and displays vividly the changes in the spectrum due to the roton-roton coupling. Namely, the coupling removes singularities in the unperturbed density of states at both roton and max-excitation thresholds, depresses the spectrum near the continuum edges, and splits off a bound state of two rotons below the two-roton continuum. Furthermore, in Fig. 5, when the max-excitation contribution is included as well, the spectrum exhibits secondary peaks within the continuum near $\epsilon \cong 0$ and $\epsilon \cong 1$, respectively. In order to estimate the observability of the secondary peaks, it is necessary to include a finite roton lifetime in the analysis. Such a calculation is presented below.

The above results, although in part restricted to the weak coupling limit, provide a refreshing insight into the physics of the formation of bound roton pairs. As the attractive interaction between excitations becomes stronger ($|\hat{g}_4|$ increases), the strength of the bound-state peak increases at the cost of depressing the density of states within the continuum.

In the preceding part of this section we have calculated the two-roton spectrum neglecting the roton lifetime associated with collision broadening. As discussed above, the calculated spectrum displays unusual structure near the edges of the continuum due to interactions between excitations. On the other hand, it is apparent that the theoretical results in Fig. 5 differ substantially from the presently available Raman data shown in Fig. 3. This discrepancy can be readily explained by including

the finite roton lifetime and keeping in mind instrumental broadening in the experiment.

To include a finite roton lifetime we proceed as above, but include in Eq. (3.7) a phenomenological parameter Γ which describes the temperature-dependent single-roton width. Thus, using Eq. (3.7) together with the unrenormalized density of Eq. (3.9), we need to evaluate

$$F(K=0, E) = 2 \left(\frac{k_0}{2\pi} \right)^2 \mu_0^{1/2} \int_0^{2D} \frac{x^{-1/2} dx}{E - x + i\Gamma} \quad (3.21)$$

for finite Γ values. Here we shall approximate Γ by an energy-independent parameter; the extension of our analysis to energy-dependent lifetimes is straightforward, but involves numerical integrations. In terms of a new variable $z = x^{1/2}$, Eq. (3.21) can be expressed in the dimensionless units [writing $\hat{f} \equiv 2F/\hat{\eta}$, where $\hat{\eta} = (k_0/\pi)^2 (\mu_0/2D)^{1/2}$] as

$$\hat{f}(K=0, E) = 2(2D)^{1/2} \int_0^{(2D)^{1/2}} \frac{dz}{E - z^2 + i\Gamma} \quad (3.22a)$$

Evaluation of Eq. (3.22a) is straightforward and gives

$$\hat{f} = \frac{(2D)^{1/2}}{\beta} \ln \left(\frac{\beta + (2D)^{1/2}}{\beta - (2D)^{1/2}} \right), \quad (3.22b)$$

where $\beta^2 \equiv E + i\Gamma$. The real and imaginary parts of Eq. (3.22) may be, respectively, expressed in the form

$$\text{Re}\hat{f} = \frac{1}{2^{1/2}\gamma} \left((\gamma + \epsilon)^{1/2} \ln \frac{(1 + \gamma^2 - 2\epsilon)^{1/2}}{1 + \gamma - [2(\gamma + \epsilon)]^{1/2}} + (\gamma - \epsilon)^{1/2} \tan^{-1} \frac{[2(\gamma - \epsilon)]^{1/2}}{-1 + \gamma} \right), \quad (3.23a)$$

$$\text{Im}\hat{f} = \frac{1}{2^{1/2}\gamma} \left((\gamma + \epsilon)^{1/2} \tan^{-1} \frac{[2(\gamma - \epsilon)]^{1/2}}{-1 + \gamma} - (\gamma - \epsilon)^{1/2} \ln \frac{(1 + \gamma^2 - 2\epsilon)^{1/2}}{1 + \gamma - [2(\gamma + \epsilon)]^{1/2}} \right), \quad (3.23b)$$

where $\gamma = (\epsilon^2 + \gamma^2)^{1/2}$ and the dimensionless energy (ϵ) and width (γ) parameters are defined above. In the limiting case of infinite roton lifetime ($\gamma \rightarrow 0$), Eqs. (3.23) reduce to the results presented in Eq. (3.11) which were previously discussed. Finally, the two-roton spectrum, including a finite roton lifetime, is given by

$$\rho_2(K=0, \epsilon) = - \frac{\hat{\eta}}{4\pi} \frac{\text{Im}\hat{f}}{[1 - \hat{g}_4 \text{Re}\hat{f}]^2 + [\hat{g}_4 \text{Im}\hat{f}]^2}; \quad (3.24)$$

the latter result is valid for positive as well as negative energy (ϵ) values.

In Fig. 6 the spectrum calculated from Eq. (3.24) is shown for various values of the roton width corresponding to different temperatures. As seen in Fig. 6, when the binding energy is larger than the

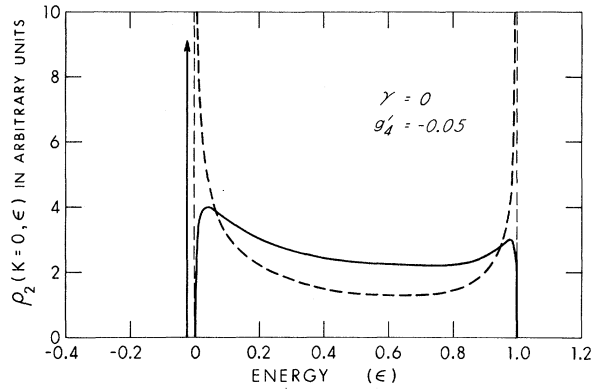


FIG. 5. Calculated joint density of states ρ_2 for two rotors with zero total momentum plotted as a function of dimensionless energy $\epsilon = (\omega - 2\Delta_0)/2D$. Dotted lines indicate the spectrum in the absence of interactions. Inclusion of an attractive roton-roton coupling removes the singularities at $\epsilon=0$ and $\epsilon=1$, shifts the spectrum to lower energies, and splits a two-roton bound state off below the two-roton continuum as shown by the solid lines. In this figure the single-roton lifetime was taken to be infinite, i. e., $\gamma=0$.

single-roton width (a situation attainable experimentally¹⁵), the peak corresponding to a bound state is well separated from the continuum. For very low temperatures, i. e., small-roton widths, three distinct peaks appear in the spectrum. As the temperature is increased, the two peaks near the bottom ($\epsilon \sim 0$) of the continuum merge, while the smaller peak near the top of the continuum ($\epsilon \sim 1$) is further depressed. Finally for large enough temperature a single asymmetric peak remains in the spectrum (see Fig. 6) in remarkable agreement with experiment.¹² Unfortunately, the experimental instrument width obscures the resolution of the bound state peak from structure within the continuum. Nevertheless further studies of the Raman spectrum of superfluid helium at lower temperatures may be able to resolve the double-peak structure discussed above. Also such Raman studies would provide very precise information concerning the roton lifetime.

We believe that the close resemblance of the calculated density of states to the experimental Raman spectrum provides strong evidence for an attractive interaction between rotors, and the existence of bound roton pairs with zero total momentum.

B. Bound States with $K \neq 0$

It is interesting to ask whether bound roton pairs with nonzero total momentum can be split off below the two-roton continuum even though the unperturbed density of states $\rho_2^{(0)}(K \neq 0)$ is nonsingular, in contrast to the $K=0$ case, but does contain a discontinuity at the bottom of the continuum as shown in the

Appendix. To investigate the formation of two-roton bound states with momentum $K \neq 0$, we calculate the spectrum in the same manner as above, but including the appropriate unrenormalized two-roton density of states. From this point on we shall not reiterate the arguments regarding the sign of the coupling, but rather pursue the theory developed in the previous sections and hence restrict attention solely to the energy region near the roton minimum.

A straightforward but tedious derivation (see the Appendix) yields the unperturbed density of states, accurate near the $2\Delta_0$ threshold energy, as

$$\rho_2^{(0)}(K \neq 0, \omega) = \mu_0 k_0^2 / 4\pi K \equiv \rho_0(K), \quad (3.25)$$

which is valid for momenta K in the range $2[\mu_0(\omega - 2\Delta_0)]^{1/2} < K \leq 2k_0$.³² With the simple expression for $\rho_0(K)$ from Eq. (3.25), which is independent of energy, it is a simple matter to express the function of Eq. (3.7) in the form

$$F(K, \omega) = 2\rho_0(K) \int_0^{2D} \frac{dx}{E - x + i\Gamma}, \quad (3.26)$$

where $E = \omega - 2\Delta_0$ and $x = \omega' - 2\Delta_0$. Performing the integration, the results for the real and imaginary parts of $F(K, \omega)$ can be expressed analytically:

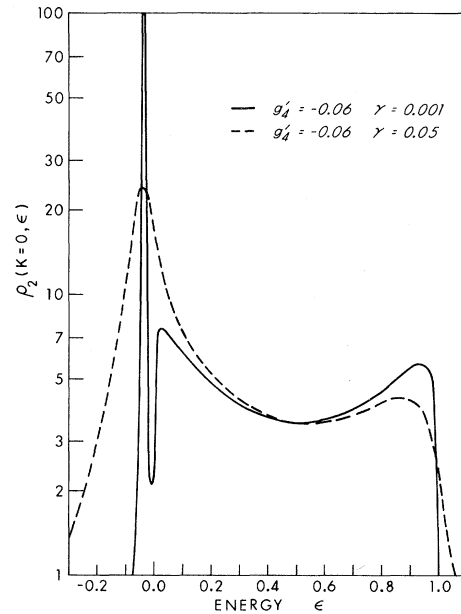


FIG. 6. Calculated joint density of states ρ_2 for two rotors with zero total momentum plotted as a function of dimensionless energy $\epsilon = (\omega - 2\Delta_0)/2D$. At low temperatures ($\gamma=0.001$ case) the two-roton bound state exhibits a sharp peak below the continuum ($\epsilon < 0$) while two secondary peaks occur in the spectrum near the energy thresholds $\epsilon=0$ and $\epsilon=1$. At higher temperatures the roton width γ increases and, as in the example $\gamma=0.05$, smears out the secondary peak structure. In the latter case the spectrum is dominated by a single peak near $\epsilon=0$ in accord with experiment.

$$\text{Re}F(K, \omega) = \rho_0(K) \ln \frac{E^2 + \Gamma^2}{(2D - E)^2 + \Gamma^2}, \quad (3.27a)$$

$$\text{Re}F(K, \omega) \simeq \rho_0(K) \ln \frac{E^2 + \Gamma^2}{4D^2}, \quad (3.27b)$$

$$\text{Im}F(K, \omega) = -2\rho_0(K) \left[\tan^{-1} \left(\frac{2D - E}{\Gamma} \right) - \tan^{-1} \left(\frac{-E}{\Gamma} \right) \right], \quad (3.27c)$$

and

$$\text{Im}F(K, \omega) \simeq -2\rho_0(K) \left[\frac{1}{2}\pi + \tan^{-1}(E/\Gamma) \right]. \quad (3.27d)$$

In the approximate expressions [Eqs. (3.27b) and (3.27d)] we have used the fact that $\Gamma \ll D$ and $|E| \ll D$, where D is the cutoff energy. The results given by Eqs. (3.27) provide a complete description of the two-particle density of states as defined in Eq. (3.5).

For simplicity we consider first the limiting case of vanishing roton width. In this instance the spectrum is especially lucid and described by the functions

$$\text{Re}F(K, \omega) = 2\rho_0(K) \ln(|E|/2D), \quad (3.28a)$$

and

$$\text{Im}F(K, \omega) = -\delta \text{ for } E < 0 \quad (3.28b)$$

$$= -2\pi\rho_0(K) \text{ for } E > 0, \quad (3.28c)$$

where it is understood that δ tends to zero. Again it is convenient to define a dimensionless quantity f via $F \equiv \rho_0(K)f$, and then obtain the total spectrum from the general form in Eq. (3.5) in terms of the f functions. In the energy region below the continuum ($E < 0$), substitution of Eqs. (3.28) into Eq. (3.5) gives

$$\rho_2(K, \omega) = (1/2g'_4)\rho_0(K)\delta[1 - 2g'_4 \ln(|E|/2D)], \quad (3.29)$$

in terms of the dimensionless coupling $g'_4 = \rho_0(K)g_4$ parameter. It is clear from Eq. (3.29) that a bound roton pair with finite total momentum will be formed below the continuum for arbitrarily small but attractive coupling. The binding energy E_B follows immediately from Eq. (3.29):

$$E_B = 2De^{-1/2|g'_4|}, \quad (3.30)$$

an expression which is analogous to the Bardeen, Cooper, and Schrieffer (BCS) theory of superconductivity.³³ The appearance of a two-roton bound state with finite momentum for arbitrarily small roton-roton interactions is related to the discontinuity in the unrenormalized two-roton density of states at the bottom of the continuum.

It is informative to rewrite Eq. (3.29) as

$$\rho_2(K, \omega) = \frac{1}{4(g'_4)^2} \rho_0(K) e^{-1/2|g'_4|} \delta \left(\frac{E - E_B}{2D} \right), \quad (3.31)$$

which exhibits the strength of the δ -function spike

in the spectrum. Note that the strength tends to zero as the coupling vanishes.

Within the continuum the interactions between excitations modifies the density of states in a spectacular way which bears little resemblance to the unperturbed density which is independent of energy. The modified spectrum follows by inserting Eqs. (3.28a) and (3.28c) into Eq. (3.5) to find

$$\rho_2(K, \omega) = \frac{\rho_0(K)}{2\pi g'_4} \frac{2\pi g'_4}{[1 - 2g'_4 \ln(E/2D)]^2 + (2\pi g'_4)^2}. \quad (3.32)$$

The latter expression exhibits a peak near the bottom of the continuum at an energy $E = |E_B|$, with a height of $h = \rho_0/[4\pi^2(g'_4)^2]$. Consequently the strength of the secondary peak within the continuum is roughly $|E_B|\rho_0/[4\pi^2(g'_4)^2]$, which is considerably smaller than the strength of the bound-state peak [from Eq. (3.31)]. These spectral features are illustrated in Fig. 7, and demonstrate how the roton-roton interaction pushes states toward lower energy and simultaneously enhances the strength of the bound-state peak.

To relate our theory to experimental data we again turn to a finite temperature-dependent single-roton width. In the present case, because of the simple unrenormalized density of states, the spectrum is obtained in analytic form using Eqs. (3.27) and (3.5). The results are plotted in Fig. 8. Note

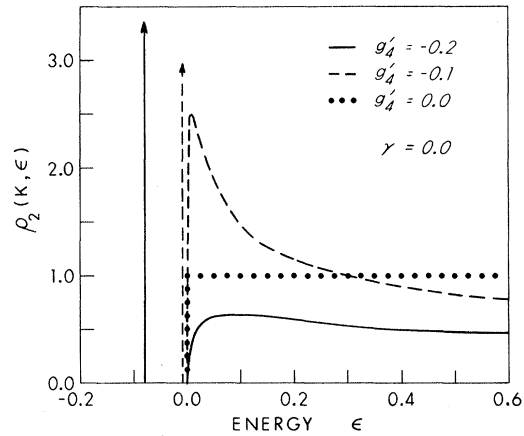


FIG. 7. Calculated density of states ρ_2 for two rotors with nonzero total momentum K plotted as a function of dimensionless energy $\epsilon = (\omega - 2\Delta_0)/2D$. Dotted lines show the spectrum without roton-roton coupling. The single-roton width γ was taken to be zero for all three curves to demonstrate vividly the formation of bound roton pairs. In the small coupling limit ($g'_4 = 0.1$) the spectrum becomes asymmetric and exhibits a δ -function peak corresponding to a bound state as shown by the dashed lines. Stronger coupling ($g'_4 = -0.2$) further depresses the density of states within the continuum ($\epsilon < 0$) and simultaneously gives rise to a bound state with increased strength and larger binding energy as shown by the solid lines.

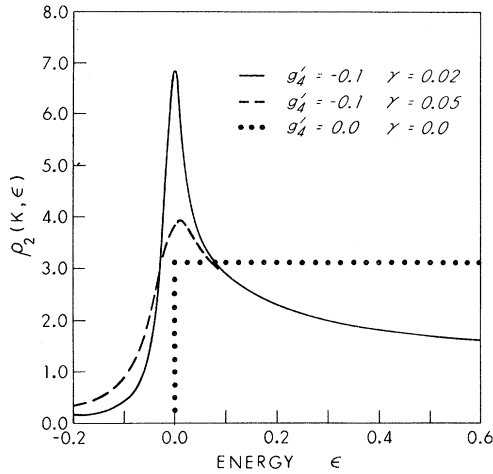


FIG. 8. Calculated two roton spectrum ρ_2 at finite total momentum including a finite single-roton width γ . The dimensionless energy is $\epsilon = (\omega - 2\Delta_0)/2D$. The dotted curve gives the unperturbed density of states, while the dashed and solid lines display the spectrum including interactions for $\gamma = 0.02$ and $\gamma = 0.05$, respectively. As a consequence of the attractive roton-roton coupling g_4' , the spectrum exhibits a sharp peak near the two-roton energy threshold ($\epsilon = 0$). In contrast to the results of Fig. 7, the finite roton lifetime broadens the peak corresponding to a bound state and thus obscures somewhat the position of the two-roton bound state.

that inclusion of the roton width shifts the bound-state peak somewhat and broadens it substantially. We shall see in Sec. IV that the broadening and energy shift associated with the roton lifetime play an important role in determining the position of the bound-state peak when the bound state hybridizes with the single-particle spectrum. If the roton width is neglected, the theoretical analysis would predict that the single-particle spectrum should bend over at energies below $2\Delta_0$ in contrast to experiment as discussed in the introduction. Because the unperturbed density $\rho_0(K)$ is inversely proportional to the total momentum, the use of a simple contact interaction model predicts a momentum dependence of the bound-state peak. We shall examine this dependence in Sec. III C.

Finally, some remarks are in order regarding experimental consequences of the preceding results for the bound state of finite momentum. As seen from Figs. 7 and 8, the secondary peak near the energy threshold $2\Delta_0$ is too small to be distinguished from the primary bound-state peak, especially since the roton lifetime smears out the structure at finite temperatures. Further, our results suggest that two-roton states with momentum $K > 2k_0$ must necessarily have energy higher than the bound states with $K < 2k_0$. Such a trend has been noticed in the neutron data¹¹ for helium, although the structure in the data is quite broad for $K > 2k_0$.

C. Bound States with Nonzero Angular Momentum

So far our theoretical analysis has been based on the oversimplified model Hamiltonian of Eq. (2.7) in which the momentum dependence of the quasiparticle scattering amplitude is neglected. As discussed in Sec. I, the model couples only s -like two-roton states and provides an incomplete description of the true roton-roton interaction. In fact, Iwamoto¹⁶ and Greytak *et al.*¹⁵ have argued that the Stephen mechanism¹³ for light scattering from superfluid helium suggests that the light interacts only with roton pairs of d -like ($l = 2$) symmetry.

Briefly we present a generalization of our model to include scattering of roton pairs with total linear momentum $K = 0$, but with arbitrary l angular momentum. Using the fact that $K = 0$, our model Hamiltonian can be generalized to

$$\mathcal{H}_4 = \frac{1}{2} \sum_{kk'} V_{kk'} a_k^\dagger a_{-k}^\dagger a_{k'} a_{-k'}, \quad (3.33)$$

with the restriction

$$V_{kk'} = V_{-kk'} = \gamma(k, -k; k', -k'). \quad (3.34)$$

In the case of rotons it is a good approximation to write $V_{kk'} = V_{k_0k'_0}$ (k_0 being the roton momentum at the energy minimum) and expand the coupling in spherical harmonics:

$$V_{k_0k'_0} = \sum_l (2l+1) g_4^l P_l(\cos\theta_{k_0k'_0}), \quad (3.35a)$$

$$V_{k_0k'_0} = \sum_l g_4^l \sum_m 4\pi Y_l^{m*}(\vec{k}_0) Y_l^m(\vec{k}'_0), \quad (3.35b)$$

where g^l stands for the coupling between states of l angular momentum and, as a consequence of the symmetry given by Eq. (3.34), only even l states are coupled. For each set of l and m values it is possible to write separate Bethe-Salpeter equations and calculate individually the spectral functions $\rho_2^l(K=0, \omega)$ which are additive contributions to the two-particle spectrum from pair states of l -type symmetry.

Without giving the details of the derivation, we note that the solution of the Bethe-Salpeter equations proceeds exactly as before and involves summation of a simple geometric series. The main modifications in the results are to change the coupling g_4 to g_4^l and replace $F(K=0, \omega)$ by $F_{lm}(K=0, \omega)$, where

$$F_{lm}(K=0, \omega) = [1/(2\pi)^3] \int d^3k \int d\vec{\omega} Y_{lm}^*(\vec{k}) \times G_1^{(0)}(k, \omega - \vec{\omega}) G_1^{(0)}(k, \vec{\omega}) Y_{lm}(\vec{k}). \quad (3.36)$$

Since the propagators $G_1^{(0)}$ have no angular dependence, the integration over solid angle Ω_k is trivial and reproduces the function $F_{lm}(K=0, \omega) = F(K=0, \omega)$ defined in Eq. (3.3). Therefore the modifications in the spectral function ρ_2 due to l -type states are included by making the replacement $g_4 \rightarrow g_4^l$, but using the same $F(K=0, \omega)$ functions which were calculated previously. Hence we conclude that bound

roton pairs with various even l values [as required by the restriction of Eq. (3.34)] may exist and give rise to sharp peaks in the ρ_2^l spectral functions at different energies corresponding to the respective bound states. It is important to stress, however, that the analytic form of the energy dependence of the theoretical two-roton spectrum is identical for all of the allowed l states. Thus a distinction between bound states of different angular momentum character requires experimental information other than the energy dependence of the spectrum, e. g., the polarization properties of the scattered light.

The depolarization ratio R ($R = I_{yx}/I_{yy}$ where $I_{\alpha\beta}$ denotes scattered intensity of light incoming with polarization α and scattered light having polarization β) of the Raman spectrum has been measured for liquid helium by Greytak and Yan.¹² Their experimental data¹² yield $R = 0.9 \pm 0.2$, whereas the Stephen theory¹³ of the light scattering predicts $R = 0.75$ for a D state in contrast to $R = 0$ for s -type states. On the basis of the depolarization data, Iwamoto¹⁶ and Greytak *et al.*,¹⁵ have argued that the bound roton pair is in a D state ($l = 2$) of angular momentum. Nevertheless it may be that S -like bound states also exist, but contribute very weakly (if at all) to the observed spectrum due to a relatively smaller light scattering amplitude from the latter states.

Furthermore, it is worth mentioning that in the case of bound roton pairs with finite total momentum, the spectrum contains admixtures of states with various angular momenta. Thus the coupling parameters g_4^l discussed above are not simply related to the coupling of rotons with finite total momentum.

IV. HYBRIDIZATION OF TWO-ROTON BOUND STATE WITH SINGLE-PARTICLE STATES

As discussed in the Introduction, the existence of bound roton pairs in a large region of momentum space suggests that a hybridization of the bound state with the single-particle spectrum should occur. An interesting consequence of such mixing would be that structure associated with the bound state would show up in the single-particle spectrum. It has already been mentioned¹⁴ that the above hybridization would split the single-particle spectrum into two branches in agreement with the neutron data.¹¹

It should be emphasized that the two-particle spectrum relates to the dynamics of two helium particles, while the single-excitation spectrum describes essentially the motion of a single helium particle. For this reason the coupling of one- and two-particle states proceeds via an intermediary particle from the zero-momentum condensate. The coupling mechanism is shown diagrammatically in Fig. 4(a), where the zig-zag line

pertains to the condensate particle and the solid lines refer to single-particle states. In other words one particle together with a condensate particle can scatter into the two-roton system. This type of interaction is represented by the model Hamiltonian in Eq. (2.13) and is characterized by a coupling parameter $g_3 = N_0^{1/2} g_4$, where g_4 is the roton-roton coupling constant and N_0 is the number of particles in the condensate.

Bound roton pairs will cause a particularly strong distortion of the single-particle spectrum. The influence of the bound states shows up in the single-particle self-energy Σ_1 as shown diagrammatically in Fig. 9. In other words, the single-particle propagator becomes

$$G_1^{-1}(K, E) = E - \Omega(K) - \Sigma_1, \quad (4.1)$$

where $\Omega(K) = E(K) - 2\Delta_0$ is the single-particle dispersion measured from the energy $2\Delta_0$ and $E(K)$ is shown in Fig. 1. Furthermore, Σ_1 is given by

$$\Sigma_1 = 2(g_3')^2 \Delta_0 f(E) / [1 - g_4' f(E)], \quad (4.2)$$

with the dimensionless quantities f and g_4' defined in the previous sections and using a dimensionless parameter $g_3' = g_3 [\rho_0(K)/\Delta_0]^{1/2}$ to describe the hybridization process.

Carrying over the results of Eqs. (3.28) for the case of zero single-particle width, the one-particle spectrum below the continuum ($E < 0$) is determined by the Green's function

$$G_1^{-1}(K, E < 0) = E - \Omega(K) - (g_3')^2 \Delta_0 \times \frac{4 \ln(|E|/2D)}{1 - 2g_4' \ln(|E|/2D)}. \quad (4.3)$$

Throughout Sec. IV we consider the roton-roton coupling to be attractive. The position of the pole in the single-particle Green's function is the solution of the equation

$$E - \Omega(K) = -2\Delta_0 \frac{(g_3')^2}{g_4'} \left[1 - \frac{1}{1 - 2g_4' \ln(|E|/2D)} \right] = -2 \frac{(g_3')^2}{(g_4')^2} \Delta_0 \left[g_4' + \left(2 \ln \frac{|E|}{E_B} \right)^{-1} \right], \quad (4.4)$$

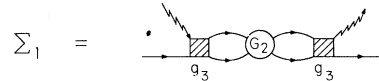


FIG. 9. Dyson equation for the single-particle self-energy Σ_1 . The propagator G_2 includes bound roton pairs and is shown in Fig. 4(b). The zig-zag lines represent particles from the condensate and the hybridization coupling is $g_3 = g_4 [N_0(T)]^{1/2}$, where $N_0(T)$ is the number of particles in the condensate.

where the expression (3.30) has been used for the binding energy E_B . At the energy given as the solution of Eq. (4.4), one gets a Dirac δ singularity in the one-particle density of states. The strength of this singularity can be calculated in a straightforward way and one obtains

$$\rho_1(K, E < 0) = \left[1 + \left(\frac{g'_3}{g'_4} \right)^2 \frac{\Delta_0}{|E|} \left(\ln \frac{|E|}{E_B} \right)^{-2} \right]^{-1} \times \delta(E - E_1(K)), \quad (4.5)$$

where $E_1(K)$ is the root of Eq. (4.4), at which energy the singularity occurs.

In order to discuss the one-particle spectral function below the characteristic energy $2\Delta_0$, it should first be mentioned that at arbitrary momentum K one gets one solution of Eq. (4.4) corresponding to a singular contribution to ρ_1 without any continuous part. In this way, below $2\Delta_0$, one branch appears, which approximately coincides with the unperturbed one-particle branch if $\Omega(K) \ll 0$, i. e., $E(K) < 2\Delta_0$. As $E(K)$ approaches and goes above $2\Delta_0$, this branch tends to the energy of the two-roton binding energy asymptotically. The strength of the singular contribution is approximately unity if the energy is far from the two-roton binding energy. However if the $E(K)$ energy is near the energy of the bound state, the strength rapidly decreases. The asymptotic form of the strength is proportional to $E(\ln E)^2$. It is worth mentioning that there is no contribution to the ρ_1 spectrum between the energies $-E_B$ and $E = 0$.

The lower branch described above has been first discussed by Pitaevskii, who in his final formulas has neglected the binding energy E_B . Carrying out this approximation our results reproduce his previous ones. On the other hand, in these publications¹⁰ the possible existence of a second branch has not been mentioned.

Continuing our discussion let us turn to the energy range $E > 0$ where the spectrum is continuous but may exhibit sharp peaks. Now we need to include both real and imaginary parts of the f function defined in Eq. (3.28) to express the single-particle propagator given by Eqs. (4.1) and (4.2):

$$G_1^{-1}(K, E > 0) = E - \Omega(K) - 2(g'_3)^2 \Delta_0 \times \frac{f(1 - g'_4 f^*)}{(1 - g'_4 \text{Re} f)^2 + (g'_4 \text{Im} f)^2}, \quad (4.6)$$

where

$$f = 2 \ln(E/2D) + 2\pi i. \quad (4.7)$$

Then the one-particle spectral function given by Eq. (2.8) can be written as

$$\rho_1(K, E > 0) = + \frac{1}{\pi} \frac{\text{Im} G_1^{-1}(K, E)}{[\text{Re} G_1^{-1}(K, E)]^2 + [\text{Im} G_1^{-1}(K, E)]^2}. \quad (4.8)$$

First we discuss some particular limits. If $E(K) \gg 2\Delta_0$ and, in the first approximation, the single-particle branch given in Fig. 1 is far from the two-roton bound state, the hybridization is weak and a strong peak is expected at the energy $E(K)$. Only the single-particle lifetime should be affected by the possible decay of the single-particle excitation into the two-particle continuum which begins at energy $E = 0$. We introduce an energy shift $\delta\Omega(K)$ as

$$\delta\Omega(K) = 2(g'_3)^2 \Delta_0 \text{Re} \frac{f(1 - g'_4 f^*)}{(1 - g'_4 \text{Re} f)^2 + (g'_4 \text{Im} f)^2}, \quad (4.9)$$

which can be taken to be independent of the energy variable E , and similarly the lifetime $\tau(K)$,

$$\frac{1}{2\tau(K)} = \text{Im} \Sigma_1 |_{E=\Omega(K)} = + \text{Im} G_1^{-1} |_{E=\Omega(K)}, \quad (4.10)$$

where Eq. (4.1) has been applied.

In terms of these functions $\rho_1(K, \omega)$ shows a Lorentzian form in the neighborhood of the single-particle peak

$$\rho_1(K, E) = \frac{1}{\pi} \frac{1/2\tau(K)}{[E - \Omega(K) - \delta\Omega(K)]^2 + (1/2\tau(K))^2}. \quad (4.11)$$

The inverse lifetime given by Eqs. (4.10) and (4.7) can be expressed in a simple form in terms of the two-particle spectral function introduced by Eq. (3.5), namely

$$1/\tau(K) = 2\pi(2g_3)^2 \rho_2(K, E = \Omega(K)), \quad (4.12)$$

where the notations $F(K, E) = \rho_0(K)f$ and $g'_3(K) = g_3 \times [\rho_0(K)/\Delta_0]^{1/2}$ have been considered. This expression of the lifetime has the form of the "Golden Rule," where $2g_3$ is the matrix element of the Hamiltonian given by Eq. (2.13) and $\rho_2(K, E)$ is the final density of states of the process in which a one-particle excitation decays into the two-roton continuum. It is obvious from this result that the width of the single-particle branch is mainly determined by the two-particle density of states.

The other interesting limit, which should be discussed separately, can be found at the threshold of the two-particle continuum $E \gtrsim 0$. If $\Omega(K) \gg E \times |\text{Im} \Sigma_1|$, that means we are far from the hybridization point, and if $|\text{Im} \Sigma_1|$ is "small" (i. e., does not exhibit a strong peak near the two-roton binding energy as in the infinite lifetime case), then one can get a simple asymptotic form for ρ_1 . In this case, $[\Omega(K)]^2$ is dominant in the denominator of the

expression (4.8). The numerator can be written in terms of $\rho_2(K, E)$ similarly to formulas (4.10) and (4.12), and we obtain

$$\rho_1(K, \omega) \sim (2g_3)^2 \rho_2(K, E) / [\Omega(K)]^2. \quad (4.13)$$

Thus if the original one-particle branch is far from the threshold, then the two-particle density of states is mixed into the one-particle spectrum, and the mixing is weaker the further ρ_2 lies from the original single-particle branch. The peak in the two-particle spectrum shown in Fig. 5 is reflected by

$$\rho_1(K, E > 0) = \frac{(g_3')^2 (g_4')^2 \Delta_0^{-1} [\pi^2 + (\ln(E/E_B))^2]}{\{[(g_4')^2 \Delta_0^{-1} (E - \Omega) - 2 |g_4'| (g_3')^2] [\pi^2 + (\ln(E/E_B))^2] + (g_3')^2 \ln(E/E_B)\}^2 + (\pi g_3')^2}, \quad (4.14)$$

where the notation given by Eq. (3.31) has been used. It is worth noting that the main approximation applied here is that we have calculated the unrenormalized two-particle density of states $\rho_2^{(0)}(K, E)$ using the parabola approximation for the dispersion curve around the roton minimum. The calculated single-particle spectrum ρ_1 from Eq. (4.14) is shown in Fig. 10 for different values of the unrenormalized single-excitation energy. In the renormalized spectrum of Fig. 10 there is a lower branch very close to the original one-particle energy for momenta close to the roton momentum. As the single-particle energy moves closer to the hybridization region, the lower branch bends over and asymptotically approaches the roton pair binding energy $E = -E_B$. In the above analysis, the lifetime of the lower branch is infinite; however the *intensity* of the lower branch decreases very rapidly as the lower peak moves nearer to the two-roton binding energy. Thus, in the latter limit, the spectrum is dominated by the resonance structure as shown in Fig. 10. On the other hand, if the single-particle branch coincides with the

the single-particle spectrum also. This hybridization can be seen in Fig. 10. It is worth mentioning that the validity of Eq. (4.13) depends only on fulfilling the assumption $|\Omega(K)| \gg |E| |\text{Im}\Sigma_1|$, so it holds for both sides of the hybridization point providing the single-roton lifetime is sufficiently short.

The general formula given by (4.8) for the one-particle density of states in the region $E > 0$ can be obtained by inserting the expression (4.7) into Eq. (4.6) and, after performing some algebra, one obtains

two-roton continuum, a peak in ρ_1 occurs near the original one-particle energy; but the latter peak is then substantially broadened. In short, as a result of the hybridization, two peaks appear in the single-particle spectrum ρ_1 : One peak corresponds to a renormalized single-particle excitation, while the other peak represents structure associated with the two-roton bound state. In the preceding analysis we have neglected the single-roton lifetime.

To provide a more reasonable description of the neutron scattering data, the theory should include a finite single-particle lifetime. Since we are primarily interested in the influence of the bound state on the spectrum, we include solely the finite single-roton lifetime which broadens the two-roton bound-state structure. The single-particle spectrum then becomes

$$\rho_1(K, E) = (-1/\pi) \text{Im} G_1, \quad (4.15)$$

with G_1 defined by Eq. (4.6) in terms of the $f(E, \Gamma)$ from Eqs. (3.28b) and (3.28d) [recall that $F = \rho_0(K)f$]. The final result for the single-particle spectrum becomes

$$\rho_1(K, E) = -\frac{1}{\pi} \text{Im} \left(E - \Omega(K) + \frac{1}{2}i\Gamma - 2(g_3')^2 \Delta_0 \frac{f(1 - g_4' f^*)}{(1 - g_4' \text{Re}f)^2 + (g_4' \text{Im}f)^2} \right)^{-1}, \quad (4.16)$$

where

$$f = \ln[(E^2 + \Gamma^2)/4D^2] - 2i \left[\frac{1}{2}\pi + \tan^{-1}(E/\Gamma) \right]. \quad (4.17)$$

The spectrum given by Eq. (4.16) is plotted in Fig. 11. The calculated spectrum shown in Fig. 11 exhibits some prominent features which are in striking accord with the neutron data: (i) Over a wide range of single-particle energies Ω (corresponding to a large span of momenta $K \cong 0.5 k_0$ to $1.2 k_0$), the *single-particle density of states exhibits two peaks—*

one which is sharp and lies below the two-roton continuum, and a broad secondary peak extending well above the two-roton threshold. (ii) As the unrenormalized single-particle energy moves closer to the two-roton continuum ($\Omega \sim 0$), there is a transfer of intensity from the sharp "single-particle" peak to the secondary structure within the continuum. (iii) When the unperturbed energy Ω overlaps with the continuum (e.g., $\Omega = 1$), the secondary peak near $E \cong 3\Delta_0$ is broader and slightly higher in energy than the structure corresponding

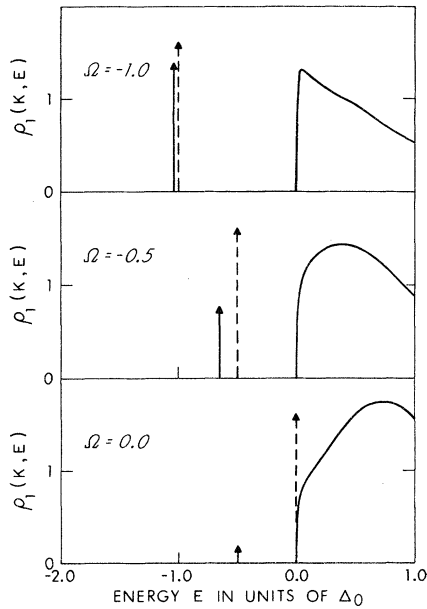


FIG. 10. Calculated single-particle spectrum ρ_1 including hybridization with two-roton bound states for various values of the single-particle energy Ω . The dotted arrows indicate the position of the *single peak* in the spectrum which would occur in the absence of coupling between excitations. Turning on the roton-roton interaction ($g_1^1 = -0.1$, $g_3^1 = 0.3$, $\gamma = 0$ for all three curves) splits the single-particle dispersion into two branches; thus *two peaks appear in ρ_1* as shown. For the choice of zero roton width considered here, the peak below the two-roton continuum is perfectly sharp, but decreases in strength as Ω approaches the continuum. The secondary peak within the two-roton continuum ($\epsilon > 0$) is broad and asymmetric in agreement with experiment.

to $\Omega = -0.5$; in the latter case the single-particle energy is well below the continuum. These three basic features of our theoretical spectrum are in

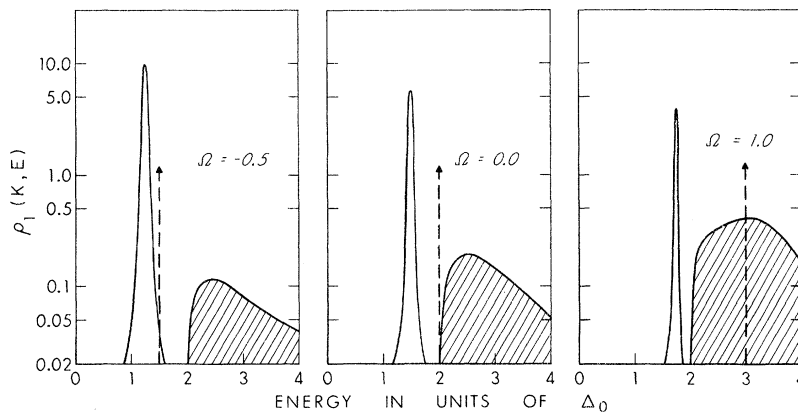


FIG. 11. Theoretical single-particle spectrum ρ_1 including a finite roton lifetime ($\gamma = 0.02$) for various values of the single-particle energy Ω . The dotted arrows show the unperturbed single-particle energies Ω ; in the zero coupling limit the spectrum would consist *only* of individual peaks at the Ω energies. The hybridization coupling ($g_1^1 = -0.1$, $g_3^1 = 0.3$ in this case) demonstrates the appearance of two new peaks in the spectrum for all three values of Ω . The peak higher in energy is broad and asymmetric in accord with the neutron data. As Ω approaches, and becomes degenerate with the two-roton continuum ($E > 2$) there is a transfer of intensity from the lower (sharper) peak to the upper branch. Note the logarithmic scale for $\rho_1(K, E)$.

remarkable agreement with the experimental neutron data.¹¹

Furthermore, our theoretical analysis explains yet another anomaly of the neutron data; namely, as the momentum of the excitation spectrum approaches $2k_0$, the sharper peak near the continuum edge $2\Delta_0$ becomes very weak and appears to penetrate into the continuum, i. e., the peak maximum seems to occur at energies slightly *larger* than twice the roton energy in contrast to previous theoretical predictions.¹⁰ This apparent anomaly is readily explained by including a finite roton lifetime in the calculation of the spectrum. First, in the vicinity of $K \sim 2k_0$, the single-particle energy is *much* higher than $2\Delta_0$; thus from the results shown in Fig. 11 and discussed above, the *strength* of the peak near $2\Delta_0$, which represents a contribution primarily from the two-roton bound state, becomes very small in accord with experiment. Then, as demonstrated in Fig. 12, at very small values of the roton width ($\gamma = 0.02$) a weak double-peak structure appears near $2\Delta_0$. As the width is increased ($\gamma = 0.1$), only a single peak appears in the theoretical spectrum at an energy very close to $2\Delta_0$. By keeping in mind instrumental broadening, it is apparent that the structure shown in Fig. 12 would show up as a very weak peak in the neutron spectrum at energies quite close to and perhaps above the two-roton energy threshold.

Finally, from Fig. 11 it is clear that the hybridization process provides a qualitative explanation of the dispersion for the anomalous upper branch in the spectrum observed by neutron scattering. Although the energy of the bound state varies with momentum K [since the unperturbed density is $\rho_0(K) \propto K^{-1}$], hybridization pushes the bound state *into* the two-roton continuum as shown in Fig. 11. Thus the single-particle spectrum displays an

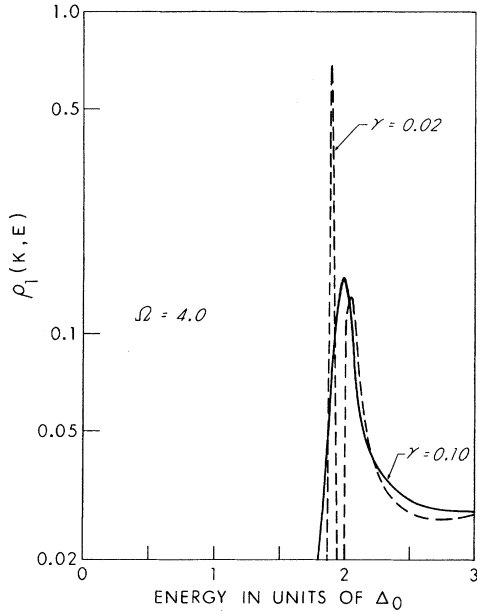


FIG. 12. Theoretical single-particle density of states ρ_1 at finite roton lifetimes as a function of energy. The unperturbed single-particle energy was taken to be large, $\Omega = 4$, corresponding to the momentum region $K \cong 2k_0$. Note that the sharp peak near $2\Delta_0$ is much weaker in intensity than the peaks in Fig. 11 although the excitation coupling is the same: $g_4^I = -0.1$, $g_3^I = 0.3$. At low temperatures (small roton width $\gamma = 0.02$) two sharp peaks appear in the spectrum as shown by the dotted lines. As the width increases to $\gamma = 0.1$ the double-peak structure is smeared out and the precise position of the single peak (solid curve) is difficult to ascertain, although it is clearly close to the two-roton threshold $E = 2\Delta_0$.

extra branch whose position in energy is determined primarily by the single-particle energy. Hence for momenta away from the roton minimum, the upper branch is pushed higher into the continuum and becomes broader. Lastly, for very small momenta, the single-particle energy is very low so that the hybridization with the two-roton bound state is very weak; therefore the upper branch near $2\Delta_0$ should not be observable at small momenta. The latter features are also in accord with the neutron data.¹¹

The theoretical results of this section suggest that further neutron scattering experiments at lower temperatures would display the hybridization process more explicitly since the coupling parameter $g_3 = g_4 [N_0(T)]^{1/2}$ is strongly temperature dependent. Also, at lower temperatures the roton lifetime would be longer and the single-particle structure associated with the bound state would become more prominent. Finally, it is worth commenting that detailed neutron studies of the hybridization process would yield the temperature dependence of $N_0(T)$, which is of considerable theoretical interest.

V. ROTON-ROTON INTERACTIONS

The true nature of roton-roton interactions is surely very complicated, especially since it relates to a residual interaction between elementary excitations (rotons) whose character resembles a moving helium particle surrounded by a backflow of other atoms. As shown by Feynman and Cohen,^{5,6} one physical mechanism for an "effective" roton-roton coupling is the phonon-exchange process discussed in the Introduction. An alternate physical description of the roton-roton scattering is to consider a phenomenological coupling derived from the "particle-backflow" description of rotons.

In the present calculation we have taken a very simple model to represent the roton-roton interaction; i. e., we assume a point interaction in real space which corresponds to a momentum-independent coupling. However we allow the coupling parameter to have different values in various momentum regions to attempt a more realistic representation of the excitation spectrum observed experimentally. In this section we relate the values of the coupling parameters which give reasonable fits to different experimental data in order to shed light on the validity of our approximations and provide clues as to the true nature of roton-roton scattering. We discuss the relevant experiments below and present estimates of the coupling parameters in Table I.

As discussed in Sec. III, the depolarization ratios for light scattered from liquid helium indicate that the primary contribution to the observed Raman spectrum arises from a bound state of two rotons with D -type angular momentum. Thus the recent measurements of the pair binding energy provides an accurate estimate of the coupling parameter $g_4^{I=2}$ defined in Eq. (3.35):

$$g_4^{I=2} = \frac{1}{2} \int V_{k_0 k'_0} P_2(\cos \theta_{k_0 k'_0}) d(\cos \theta_{k_0 k'_0}), \quad (5.1)$$

where P_2 is a Legendre polynomial whose argument $\theta_{k_0 k'_0}$ is the angle between the scattered rotons. In addition the Raman studies³⁴ yield a very accurate estimate of the single-roton lifetime which is primarily responsible for the broadening of the bound-state peak. The single-roton width can be extracted from the Raman data by convoluting the spectral function for two interacting rotons [defined in Eq. (3.24)] with the instrumental broadening profile as discussed by Greytak and Yan.³⁴ However, it is important to note that the single-roton width includes contributions from scattering processes at finite total momentum which represent an admixture of S -type and D -type, etc., coupling parameters. As a first approximation it is useful to estimate the value of a single S -like coupling param-

TABLE I. Values of the roton-roton coupling parameter g_4 in units of 10^{-38} erg cm^3 as taken from comparison of our theory to various experiments.

Experiment	g_4
Raman scattering; measurement of binding energy of roton pair (Ref. 15)	$g_4^{I=2} = -0.12$
Raman data for single-roton lifetime (Ref. 37).	$ g_4(\text{LK}) = 2.4$
Neutron scattering; position of bound state peak (Ref. 11)	$g_4 = -0.3$
Neutron studies of hybridization; Sec. IV (Ref. 11) (taking $N_0 = 0.1$).	$ g_4 = 0.85$
Viscosity data (Ref. 4).	$g_4(\text{LK}) = 2.6$

eter $g_4^{I=0}$ from analysis of the roton lifetime using the theory of Landau and Khalatnikov (LK).⁴ However, it is important to stress that their theory is restricted to second-order perturbation theory which is surely inadequate in view of the existence of bound roton pairs. Estimates of the above coupling parameters are given in Table I.

To relate our theory to neutron scattering studies is somewhat problematic since neutrons sample the density-density correlation function $S(K, \omega)$ which is not related in a simple way to the single-particle spectrum $\rho_1(K, \omega)$ which we have calculated. However, very useful information regarding the roton coupling may be obtained from neutron data by noting that $\rho_1(K, \omega)$ and $S(K, \omega)$ exhibit peaks at the *same* energy. Furthermore, a crude comparison of structure in ρ_1 with the observed spectrum yields information about the strength of the roton-roton coupling in various momentum regions.

The existence of two-roton resonances with non-zero total momentum gives rise to structure in the neutron data related to the strength of the coupling constant,

$$g_4(K) \approx \gamma(k_0, K - k_0, k'_0, K - k'_0), \quad (5.2)$$

where $|K - k_0| \sim |K - k'_0| \sim k_0$. Thus a crude estimate of $g_4(K)$ can be obtained from the strength and position of the peaks in the neutron data corresponding to two-roton resonances.

Another clue to the strength of the roton-roton coupling is provided by the hybridization of the resonance with the single-particle spectrum which is probed by neutron scattering.^{11,14} In this case the relevant coupling is

$$g_3(K) \sim g_4(K) [N_0(T)]^{1/2} \sim \gamma(0, k, k', k - k'), \quad (5.3)$$

with $|k'| \sim |k - k'| \sim k_0$, and $N_0(T)$ representing the temperature-dependent number of particles in the condensate. Here the estimate of $g_4(K)$ is hampered by uncertainty in the value of $N_0(T)$.

Other experiments which provide an estimate of

the roton lifetime include viscosity data,⁸ neutron, and light scattering studies. The neutron measurements provide a direct probe of the *single*-roton lifetime but are quite limited in accuracy due to instrumental broadening. The analysis of the viscosity data in terms of the LK theory has been carried out,⁴ but must be interpreted with care because the formation of resonances casts doubt on the validity of the LK theory of the roton lifetime. Also the relation of the viscosity to the roton lifetime may be more complicated than suggested by the simple point interaction model for the roton-roton coupling invoked by LK. It appears at present that the most accurate determination of the single-roton lifetime is possible by Raman scattering. However, the light samples only the second-order spectrum which involves roton pair excitations. Therefore the light scattering experiments do not provide a *direct* measure of the *single*-roton lifetime.

As discussed in Sec. III A, our theoretical analysis using a *constant* single-roton width as a phenomenological parameter provides a remarkably good description of the observed Raman spectrum.¹⁵ However an extension of the roton lifetime theory³⁵ including possible resonances shows that resonances can give rise to a strongly energy-dependent roton self-energy. The analysis of the Raman spectrum using the more complete calculation of the roton lifetime will be presented elsewhere.³⁵ It is worth noting a few results of the roton lifetime analysis³⁵ insofar as they provide insight into the roton-roton interaction. The previous theory⁴ of the roton lifetime based on second-order perturbation theory includes with equal importance the contribution to the lifetime from scattering processes with various momentum transfers. In contrast to the latter conclusion, the lifetime theory³⁵ including resonances suggests that scattering processes with *large* total momentum dominate the scattering contributions to the roton lifetime.

Cohen and Feynman⁶ have suggested that the roton-roton coupling can be induced by exchange of a phonon in a manner reminiscent of the BCS theory.³³ Using a deformation potential type of approach for the roton-phonon coupling and neglecting momentum dependent terms in the coupling, Cohen and Feynman estimated the roton coupling from the variation of the roton energy with respect to pressure which was known from experiment. Thereby they obtain an estimate of $g_4^{\text{CF}} = -1.3 \times 10^{-38}$ erg cm^3 . The latter estimate of the coupling is valid only for coupling of two rotons with nearly parallel momentum, since the deformation potential approach is valid for small momentum transfers.

Summarizing the results of this section, the phonon-exchange mechanism seems to play an im-

portant role in determining the roton-roton coupling, especially for nearly forward scattering of two rotons. The latter processes are most important³⁵ in determining the roton lifetime and therefore it is gratifying that the Cohen-Feynman estimate of g_4 is consistent both in sign and magnitude with our estimates for $g_4(K)$ given in Table I. From Eq. (5.1) it is apparent that the coupling $g_4^{l=2}$, for total momentum near zero, involves an average over the angle $\theta_{k_0k'_0}$. Thus it is reasonable that $g_4^{l=2}$ should be an order of magnitude *smaller* than the Cohen-Feynman estimate in agreement with experiment.

It is not surprising that the coupling of rotons bears little resemblance to the interatomic helium potential. Nevertheless, it is curious to note that the relative importance of roton scattering processes with large total momentum (as discussed above) cannot be related to the interatomic potential since the hard-core portion of the potential would strongly influence forward scattering processes with nearly zero total momentum.

Another approach to understanding the roton-roton interaction is to construct a phenomenological model for the coupling based on the influence of the backflow. Such an approach has been employed³⁶ to calculate the scattering of two He³ quasiparticles in liquid He³-He⁴ mixtures, and suggests that the backflow terms give rise to a strongly momentum-dependent coupling.

In this section we have seen that the phonon-exchange mechanism for the roton-roton coupling provides a *qualitative* understanding for the coupling parameters taken from various experiments. However, more detailed theoretical analysis of both the phonon-exchange and the backflow mechanisms as well as further experimental efforts are needed in order to understand the physical origin of the roton-roton interaction.

VI. CONCLUSIONS

We have shown that the formation of two-roton bound states can modify the excitation spectrum of superfluid helium in an essential way. The existence of such bound states provides a simple physical explanation for the discrepancies between the excitation spectrum originally proposed by Landau and the spectrum observed experimentally.

The anomalous features of the light scattering experiments on liquid helium have been resolved in a natural way by taking into account interactions between excitations. Coupling of rotons gives rise to bound pairs which exhibit a sharp peak in the two-roton spectrum at an energy below the two-roton continuum. The energy dependence of the spectrum is of the same form for bound states with different angular momentum character. Our calculated spectrum gives good agreement with the observed Ra-

man data. However, further analysis of the light coupling to liquid helium is needed to determine whether both *s*- and *d*-type bound states can occur: The light polarization data suggest that the major contribution to the observed Raman spectrum arises from bound pairs in *d*-type angular momentum states. On the other hand, there is no *a priori* reason to expect that *only d*-type pairs exist. Further Raman scattering experiments at lower temperatures would provide considerable insight into the formation of bound roton pairs. As the temperature is lowered, the structure associated with bound states becomes much sharper since the roton lifetime becomes longer. In the present paper we have followed LK in using a phenomenological energy-independent roton lifetime. The existence of resonances in the two-roton scattering requires a more thorough analysis of the single-roton lifetime which may turn out to be strongly energy dependent. Thus careful studies of the temperature dependence of the Raman spectrum from liquid helium would provide valuable information concerning the temperature variation of the roton lifetime which would reflect the calculated energy dependence of the lifetime.

Further neutron studies of liquid helium are necessary in order to determine the extent to which the bound states hybridize with the single-particle spectrum. Of particular interest is the behavior of the heretofore unexplained "extra" branch in the spectrum above $2\Delta_0$, i. e., greater than twice the single-roton energy. We have shown that the formation of two-roton resonances splits the single-particle spectrum into two branches near $2\Delta_0$ and thus provides a simple physical explanation for the "extra" branch in terms of quantum-mechanical level repulsion (hybridization). Experimental information about the extra branch would give valuable information in regard to the strength of the roton-roton coupling in various momentum regions. Furthermore, neutron data in the vicinity of the extra branch would provide an estimate of the temperature-dependent number of particles in the condensate $N_0(T)$ which plays an important role in the hybridization process, and whose value is of considerable theoretical interest.

Another manifestation of roton-roton interactions is the renormalization of the roton energy which is strongly temperature dependent. One source of renormalization is the hybridization process discussed in Sec. IV. It is clear that hybridization of the resonance with single-roton states *lowers* the single-roton energy, thus in part removing the discrepancy between the Feynman-Cohen excitation spectrum and the experimentally observed energy as shown in Fig. 2. However, there are a number of other scattering processes which contribute to the roton renormalization; the latter processes pose

an interesting theoretical challenge which lies beyond the scope of the present paper.

Our results indicate that light and neutron scattering experiments on superfluid helium at various pressures should reveal fascinating information about the excitation spectrum. It is already known that the roton energy depends strongly on pressure. Thus an analysis of the bound-state structure and, in particular, the hybridization process at various pressures would be of considerable interest from both the experimental and theoretical points of view. Such experiments may determine to what extent the phonon-exchange mechanism dominates the roton-roton scattering insofar as the latter physical mechanism predicts a variation of the coupling with changes in the roton energy with respect to pressure. Changing the roton-roton coupling by varying the pressure would result in a change in the binding energy of coupled roton pairs in various momentum regions and, at the same time, modify the hybridization of the bound state with the single-particle spectrum. Providing that the coupling is sufficiently enhanced, it may be possible to observe the double-peak structure near the two-roton energy threshold as discussed in the text.

According to our simple theory, the existence of the Bore condensed phase is important for the hybridization $g_3 \neq 0$. Above the transition temperature the hybridization and the two branches structure of the spectrum should disappear, which must be observable in experimental data.

An essential feature of our analysis is the inclusion of a finite roton lifetime in the calculation of the excitation spectrum. By starting with the excitation spectrum proposed by Landau (see Fig. 2) as the appropriate unrenormalized spectrum, we have demonstrated how the formation of two-roton resonances at finite momentum gives rise to quite unusual structure in the single-particle spectrum near $2\Delta_0$, i. e., near the resonance energy. By including the roton lifetime we have demonstrated why the spectrum observed by neutron scattering contains a peak at an energy greater than $2\Delta_0$ in contrast to predictions of other theories.^{10,25}

Our theoretical development suggests that the momentum dispersion of the two-roton bound state should be relatively smooth as a consequence of the threshold in energy in the unrenormalized two-roton density of states. Thus the hybridization of the resonance with single-particle excitations seems to be primarily responsible for the unusual momentum dependence of the resonance structure observed by neutron scattering experiments and shown in Fig. 2.

Finally, it is worth mentioning that the present paper has demonstrated the necessity of using a strongly momentum-dependent roton-roton coupling in order to achieve a qualitative understanding of

various experimental results for superfluid helium. These conclusions point out the need for further theoretical analysis of the roton-roton coupling which is essential to an understanding of the superfluid helium excitation spectrum in terms of fundamental microscopic principles.

ACKNOWLEDGMENTS

It is a pleasure to thank I. Tüttó for checking various aspects of the present paper. We have greatly benefited from stimulating discussions with J. Bardeen, G. Baym, V. Celli, M. Cohen, M. H. Cohen, R. J. Donnelly, L. M. Falicov, M. Fowler, M. Fullenbaum, T. Greytak, E. P. Gross, K. Huang, D. Pines, M. Stephen, N. R. Werthamer, and A. D. B. Woods. Also we are very grateful to F. Iwamoto for sending us a report of his work prior to publication.

APPENDIX: TWO-ROTON DENSITY OF STATES

The calculation of the joint density of states for a pair of rotons with arbitrary total momentum is straightforward but somewhat tedious. In this appendix we present the salient features of the derivation, beginning with the standard expression for the unperturbed density of states from Eq. (3.6),

$$\rho_2^{(0)}(K, \omega) = \frac{1}{2(2\pi)^3} \int d^3k \delta(\omega - \epsilon_k - \epsilon_{K-k}), \quad (\text{A1})$$

where the factor of $\frac{1}{2}$ takes into account the roton indistinguishability. Writing the momentum integrals in terms of polar coordinates by introducing the angle θ between the total momentum K and the momentum of one of the two rotons, and making use of the roton dispersion formula Eqs. (3.8a) and (3.8b), one can transform the two-roton density into the form

$$\rho_2^{(0)}(K, \omega) = [\mu_0 / (2\pi)^2] \int k^2 dk \int_{-1}^1 dx \delta(2\mu_0(\omega - 2\Delta_0) - (k - k_0)^2 - [(K^2 + k^2 - 2xkK)^{1/2} - k_0]^2) \quad (\text{A2})$$

using $x = \cos\theta$. Let us denote the root of the expression under the Dirac δ function by $x = x_0(k, K)$; then in Eq. (A2) the integral with respect to the x variable can be performed to give

$$\rho_2^{(0)}(K, \omega) = \frac{1}{8\pi^2} \frac{\mu_0}{K} \sum_i \int_{k_{\min}^i}^{k_{\max}^i} dk k \times \frac{[K^2 + k^2 - 2Kkx_0(k, K)]^{1/2}}{[2\mu_0(\omega - 2\Delta_0) - (k - k_0)^2]^{1/2}}, \quad (\text{A3})$$

where (k_{\min}^i, k_{\max}^i) stand for the momentum intervals in which the cosine function denoted by x takes real values lying between -1 and 1 . The index i labels the different intervals. The first step of the cal-

ulation is to find the roots denoted by $x_0(k, K)$ and the corresponding momentum intervals. The angle $x_0(k, K)$ is the solution of the equation

$$2\mu_0(\omega - 2\Delta_0) - (k - k_0)^2 - [(K^2 + k^2 - 2kKX_0)^{1/2} - k_0]^2 = 0. \quad (\text{A4})$$

Considering this equation for the roots $x_0(k, K)$, the two-rotors density of states given by Eq. (A3) can be transformed into a simpler form

$$\rho_2^{(0)}(K, \omega) = \frac{\mu_0}{8\pi^2 K} \sum_i \int_{k_{\min}^i}^{k_{\max}^i} k dk \times \left(\pm 1 + \frac{k_0}{[2\mu_0(\omega - 2\Delta_0) - (k - k_0)^2]^{1/2}} \right), \quad (\text{A5})$$

where the \pm correspond to different roots of Eq. (A4).

The requirement that x_0 should be real yields the following necessary restrictions for the ends of the intervals:

$$k_0 - [2\mu_0(\omega - 2\Delta_0)]^{1/2} \leq k_{\min, \max}^i \leq k_0 + [2\mu_0(\omega - 2\Delta_0)]^{1/2}, \quad (\text{A6})$$

which follows from Eq. (A4) immediately.

To obtain conditions for finding x corresponding to real angles θ , four regions of the total momentum K should be considered separately.

$$\text{Case A: } K \leq [2\mu_0(\omega - 2\Delta_0)]^{1/2}$$

Let us start with the boundary conditions as $x_0(k, K) = \pm 1$, and write $k_{x_0=1} = 1$ as the solution of Eq. (A5) for $x_0(k, K) = 1$. This equation may have two different types of solutions. In the first case the square root has the value $k - K$, while in the second case $K - k$, depending on whether $k > K$ or $K > k$. Discussing the first case, one gets two roots:

$$k_{x_0=1}^{(1), (2)} = k_0 + \frac{1}{2}K \pm \frac{1}{2}[2\alpha - K^2]^{1/2}, \quad (\text{A7})$$

where the notation $\alpha = 2\mu_0(\omega - 2\Delta_0)$ is introduced. This is the case for small enough total momentum K . Furthermore, discussing the second case, one obtains two other roots:

$$k_{x_0=1}^{(1), (2)} = \frac{1}{2}K \pm 2^{-3/2} [2\alpha - (2k_0 - K)^2]^{1/2}, \quad (\text{A8})$$

which are real if $K > 2k_0 - (2\alpha)^{1/2}$, i. e., at large enough total momentum.

Similarly, for the condition $x_0(k, K) = -1$, the following two boundary values are defined:

$$k_{x_0=-1}^{(1), (2)} = k_0 - \frac{1}{2}K \pm \frac{1}{2}(2\alpha - K^2)^{1/2}, \quad (\text{A9})$$

but now we get only one set of the solutions.

In this region the two momentum intervals labeled by + and - are illustrated in Fig. 13 by the solid lines and they represent $(k_{\min}^{(1)}, k_{\max}^{(1)})$ and $(k_{\min}^{(2)}, k_{\max}^{(2)})$. Performing the integrations in the expression given by Eq. (A5) and considering the intervals deter-

mined by the values yielded by Eq. (A7), one can obtain the final result

$$\rho_2^{(0)}(K, \omega) = \frac{\mu}{8\pi^2 K} \left\{ 2k_0^2 \left(\arcsin \left[\frac{K\alpha^{-1/2}}{2} + \frac{1}{2} \left(\frac{2\alpha - K^2}{\alpha} \right)^{1/2} \right] - \arcsin \left[-\frac{K\alpha^{-1/2}}{2} + \frac{1}{2} \left(\frac{2\alpha - K^2}{\alpha} \right)^{1/2} \right] \right) + K(2\alpha - K^2)^{1/2} \right\}. \quad (\text{A10})$$

In the limit $K \rightarrow 0$ this result reduces to the special expression discussed before and given by Eq. (3.9). Finally, we mention that in case A the necessary condition written in the form of Eq. (A6) does not affect the two integration intervals.

$$\text{Case B: } [2\mu_0(\omega - 2\Delta_0)]^{1/2} \leq K \leq [4\mu_0(\omega - 2\Delta_0)]^{1/2}$$

As we can see in Fig. 13, the integration paths illustrated by the broken lines are limited by the necessary condition given by Eq. (A6) at the energy values $k = k_0 - \alpha^{1/2}$ and $k = k_0 + \alpha^{1/2}$, respectively. On the other hand, both paths labeled by + and - are running out of the interval $-1 < x_0 < +1$ and later they are turning back. Those momentum values at which the $x_0 = \pm 1$ lines are crossed are yielded by Eqs. (A7) and (A8). In this way there are four intervals, two labeled by "+,"

$$(k_0 - \alpha^{1/2}, k_{x_0=1}^{(2)}), \quad (k_{x_0=1}^{(1)}, k_0 + \alpha^{1/2}); \quad (\text{A11})$$

and two by "-,"

$$(k_0 - \alpha^{1/2}, k_{x_0=-1}^{(2)}), \quad (k_{x_0=-1}^{(1)}, k_0 - \alpha^{1/2}). \quad (\text{A12})$$

In these intervals the integrals given by Eq. (A5) can be calculated in a straightforward way and the following result is obtained:

$$\rho_2^{(0)}(K, \omega) = \frac{\mu}{8\pi^2 K} \left\{ 2\pi k_0^2 + K(2\alpha - K^2)^{1/2} + 2k_0^2 \left[\sin^{-1} \left(\frac{K\alpha^{-1/2}}{2} - \frac{(2\alpha - K^2)^{1/2}}{2\alpha^{1/2}} \right) \right] \right\}$$

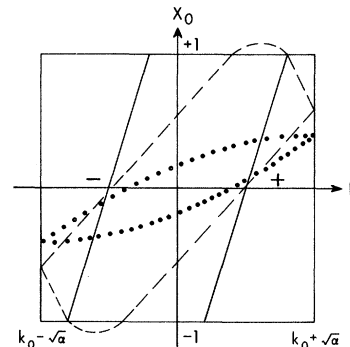


FIG. 13. Schematic representation of the integration paths in the evaluation of the unperturbed joint density of states as discussed in the Appendix.

$$-\sin^{-1}\left(\frac{K\alpha^{-1/2}}{2} + \frac{(2\alpha - K^2)^{1/2}}{2\alpha^{1/2}}\right)\Bigg\}. \quad (\text{A13})$$

Case C: $2k_0 - [4\mu_0(\omega - 2\Delta_0)]^{1/2} > K > [4\mu_0(\omega - 2\Delta_0)]^{1/2}$

In this case, the momentum values at which the absolute value of the cos would be larger than unity are complex as can be seen from Eqs. (A7) and (A8). Therefore, the two integration paths illustrated in Fig. 13 by dotted lines do not cross the $x_0 = \pm 1$ lines. In this case we have a simple situation, where the paths are limited by the momentum values $k = k_0 - \alpha^{1/2}$ and $k = k_0 + \alpha^{1/2}$ given by Eq. (A6). In these intervals the integral in Eq. (A5) can be performed and one obtains

$$\rho_2^{(0)}(K, \omega) = (\mu_0/4\pi)(k_0^2/K)H(\omega - 2\Delta_0), \quad (\text{A14})$$

i. e., the density of states is given by a simple step

Heaviside function H , which is unity when $\omega > 2\Delta_0$ and zero otherwise.

Case D: $K > 2k_0 - [4\mu_0(\omega - 2\Delta_0)]^{1/2}$

In case C, Eq. (A7) does not yield any real solutions of Eq. (A4), and therefore the paths do not intersect the line $x_0 = 1$ in the upper part of Fig. 13. This situation may change at large total momentum where the result given by Eq. (A7) does not hold any more and there is another set of solutions. The condition for appearance of these other solutions determines the fourth region discussed now. In this region one of the curves intersect the line $x_0 = 1$ twice. We do not go into the details here; it is only mentioned that the threshold of the unperturbed two-roton spectrum becomes larger than the energy of two free rotons at these very large momentum values.

*Research supported in part by the Center for Advanced Studies at the University of Virginia.

†Permanent address.

¹L. D. Landau, *J. Phys. USSR* **5**, 71 (1941); **11**, 91 (1947).

²R. J. Donnelly, *Experimental Superfluidity* (Chicago U. P., Chicago, 1967), and references cited therein.

³L. D. Landau and I. M. Khalatnikov, in *Collected Papers of L. D. Landau*, edited by D. Ter Haar (Gordon and Breach, New York, 1967), pp. 494 and 511.

⁴I. M. Khalatnikov, *Theory of Superfluidity* (Benjamin, New York, 1965), p. 47.

⁵R. P. Feynman, *Phys. Rev.* **94**, 262 (1954); R. P. Feynman and M. Cohen, *ibid.* **102**, 1189 (1956).

⁶M. Cohen and R. P. Feynman, *Phys. Rev.* **107**, 13 (1957).

⁷The momentum-dependent terms in the roton-roton interaction may be of the same order as the δ -function component as discussed in Ref. 5.

⁸K. R. Atkins and M. H. Edwards, *Phys. Rev.* **97**, 1429 (1955).

⁹A. D. B. Woods, in *Quantum Fluids*, edited by D. F. Brewer (North-Holland, Amsterdam, 1966), p. 242, and references cited therein.

¹⁰L. P. Pitaevskii, *Zh. Eksperim. i Teor. Fiz.* **36**, 1168 (1959) [*Sov. Phys. JETP* **9**, 830 (1959)]; *Usp. Fiz. Nauk* **88**, 409 (1966) [*Sov. Phys. Usp.* **9**, 197 (1966)].

¹¹A. D. B. Woods and R. A. Cowley, *Symposium on Neutron Inelastic Scattering*, Copenhagen, 1968 (unpublished); *Can. J. Phys.* **49**, 177 (1970).

¹²T. J. Greytak and James Yan, *Phys. Rev. Letters* **22**, 987 (1969). The possibility of observing rotons by Raman scattering was suggested by J. W. Halley, *Phys. Rev.* **181**, 338 (1969).

¹³M. J. Stephen, *Phys. Rev.* **187**, 279 (1969). The analogous scattering in solid helium has been considered by N. R. Werthamer, *ibid.* **185**, 348 (1969).

¹⁴J. Ruvalds and A. Zawadowski, *Phys. Rev. Letters* **25**, 333 (1970).

¹⁵T. J. Greytak, R. Woerner, J. Yan, and R. Benjamin, *Phys. Rev. Letters* **25**, 1547 (1970).

¹⁶F. Iwamoto, *Progr. Theoret. Phys. (Kyoto)* **44**, 1135 (1970).

¹⁷M. Wortis, *Phys. Rev.* **132**, 85 (1963); J. Janus, *Phys. Rev. Letters* **11**, 336 (1963).

¹⁸M. H. Cohen and J. Ruvalds, *Phys. Rev. Letters* **23**, 1378 (1969).

¹⁹E. Fermi, *Z. Physik* **71**, 250 (1931).

²⁰R. Silbergliitt and A. Brooks Harris, *Phys. Rev.* **174**, 640 (1968).

²¹J. F. Scott, *Phys. Rev. Letters* **21**, 907 (1968).

²²J. Ruvalds and A. Zawadowski, *Phys. Rev. B* **2**, 1172 (1970).

²³J. Ruvalds, *Phys. Rev. B* **3**, 3556 (1971).

²⁴L. P. Pitaevskii, *Zh. Eksperim. i Teor. Fiz. Pis'ma v Redaktsiyu* **12**, 118 (1970) [*Sov. Phys. JETP Letters* **12**, 82 (1970)].

²⁵F. Iwamoto, *Progr. Theoret. Phys. (Kyoto)* **44**, 1121 (1970).

²⁶T. Soda, K. Sawada, and T. Nagata, *Progr. Theoret. Phys. (Kyoto)* **44**, 860 (1970).

²⁷S. T. Belyaev, *Zh. Eksperim. i Teor. Fiz.* **34**, 417 (1958) [*Sov. Phys. JETP* **7**, 289 (1958)].

²⁸A. A. Abrikosov, L. P. Gorkov, and I. E. Dzyaloshinski, *Methods of Quantum Field Theory in Statistical Physics* (Prentice-Hall, Englewood Cliffs, N. J., 1963).

²⁹A. Miller, D. Pines, and P. Nozieres, *Phys. Rev.* **127**, 1452 (1962).

³⁰See, for example, P. Nozières and D. Pines (unpublished). In the event that $Z_1(k) \neq 1$, our calculation would be modified by a renormalization of the roton-roton coupling.

³¹A repulsive interaction could produce a bound state above the two-excitation continuum and give rise to a sharp peak in the spectrum above the two max-excitation energy. Such a peak is not observed experimentally.

³²As corrected in an erratum [*Phys. Rev. Letters* **25**, 632E (1970)], the unrenormalized density of states η in Ref. 14 should be $\eta = 2\rho_0(K)$ in the present notation.

³³J. Bardeen, L. N. Cooper, and J. R. Schrieffer, *Phys. Rev.* **106**, 162 (1957); **108**, 1175 (1957).

³⁴T. J. Greytak and James Yan, in *Proceedings of the Twelfth International Conference on Low-Temperature Physics*, Kyoto, 1970 (unpublished).

³⁵J. Solana, V. Celli, J. Ruvalds, and A. Zawadowski (to be published).

³⁶W. L. McMillan, Phys. Rev. **182**, 299 (1969).

³⁷Our values of the coupling are larger than those quoted by Khalatnikov in Ref. 4 by a factor of 1.414. This

factor arises by using the corrected density of states for two rotons; the Khalatnikov result for the density contains an erroneous factor of 2.

Vertex Correction Contribution to the Decay Rate of Concentration Fluctuations in Binary Liquid Critical Mixtures*

Shih-Min Lo and Kyozi Kawasaki

Department of Physics, Temple University, Philadelphia, Pennsylvania 19122

(Received 2 June, 1971)

Recently, a self-consistent scheme for the mode-mode coupling theory of critical fluctuations was developed by Kawasaki in which the decay rate of concentration fluctuations for a binary critical mixture was obtained in the simplest approximation of ignoring all the vertex corrections. In this paper we calculate the contribution of the simplest vertex corrections. We find that the corrections are 2.44% for $q \ll \kappa$, and 0.40% for $q \gg \kappa$, where q and κ are the wave number and the inverse correlation range of concentration fluctuations, respectively.

I. INTRODUCTION

The physical ideas of mode-mode coupling in critical phenomena were perhaps first introduced by Fixman,¹ who considered the critical behavior of shear viscosity in a binary mixture. The idea was reformulated in the language of a time-correlation function by Kawasaki.² Later, Kadanoff and Swift³ developed a formalism for transport coefficients, which can be given a schematic interpretation. In these theories couplings among hydrodynamic fluctuations play a crucial role in determining the macroscopic behavior of the system. Recently this formalism had been further extended⁴ with the aid of a generalized Langevin equation due to Mori⁵ in which kinetic equations obeyed by critical fluctuations are derived. A main result of the theory is the Dyson-type self-consistent equations for the time correlations of critical fluctuations of the following form:

$$G_{\vec{q}\alpha}(t) = G_{\vec{q}\alpha}^0(t) + \int_0^t dt_1 \int_0^{t_1} dt_2 G_{\vec{q}\alpha}^0(t-t_1) \times \Sigma_{\vec{q}\alpha}(t_1-t_2) G_{\vec{q}\alpha}(t_2), \quad (1.1)$$

where $G_{\vec{q}\alpha}(t) \equiv \langle a_{\vec{q}\alpha}(t) a_{\vec{q}\alpha}^\dagger(0) \rangle / \langle a_{\vec{q}\alpha} a_{\vec{q}\alpha}^\dagger \rangle$ is the renormalized propagator for the gross variable $a_{\vec{q}\alpha}$ with a wave vector \vec{q} , $\Sigma_{\vec{q}\alpha}(t_1-t_2)$ is the proper "self-energy," and $G_{\vec{q}\alpha}^0(t)$ is the unperturbed propagator obtained by ignoring coupling among hydrodynamic modes.

By introducing a renormalized vertex represented by a heavy dot \bullet , a corresponding graphical equation for $G_{\vec{q}\alpha}(t)$ is given in Fig. 1, where the renormalized correlation function $U_{\vec{q}\alpha}(t)$ is given by

$$U_{\vec{q}\alpha}(t) \equiv \langle a_{\vec{q}\alpha}(t) a_{\vec{q}\alpha}^\dagger(0) \rangle. \quad (1.2)$$

The theory has been applied, among others, to the order parameter dynamics of binary liquid critical mixtures, as well as of fluids near the liquid-gas critical point, and excellent agreement with the recent light scattering experiments⁶ has been achieved throughout the hydrodynamic and critical regimes. However, this particular calculation ignores all the vertex corrections in the equation shown in Fig. 1. Since the expansion in terms of renormalized propagators⁴ contains no obvious small parameter of expansion, there is no *a priori* reason to ignore vertex corrections, and as it stands, a possibility can not be excluded that the excellent agreement with experiments could be fortuitous. Thus it is important to examine the effects of vertex corrections to the order parameter dynamics. A calculation of the contribution of the simplest vertex correction, in the case of a binary fluid mixture, will be presented in Sec. II.

II. CALCULATIONS AND RESULTS

According to the rules given in Ref. 4, the simplest vertex corrections for Fig. 1 are found to be of the type shown in Fig. 2. Note that there all the vertex renormalizations to the vertices at each corner of the "triangles" in the right-hand side of Fig. 2 are ignored. The unperturbed propagator $G_{\vec{q}\alpha}^0(t)$ is given by

$$G_{\vec{q}\alpha}^0(t) = \theta(t) e^{(i\omega_{\vec{q}\alpha} - \gamma_{\vec{q}\alpha})t}, \quad (2.1)$$

where

$$\theta(t) = \begin{cases} 1, & t \geq 0 \\ 0, & t < 0 \end{cases} \quad (2.2)$$

and $\omega_{\vec{q}\alpha}$ and $\gamma_{\vec{q}\alpha}$ are the frequency and damping constant of the mode $a_{\vec{q}\alpha}$ in the absence of interactions